

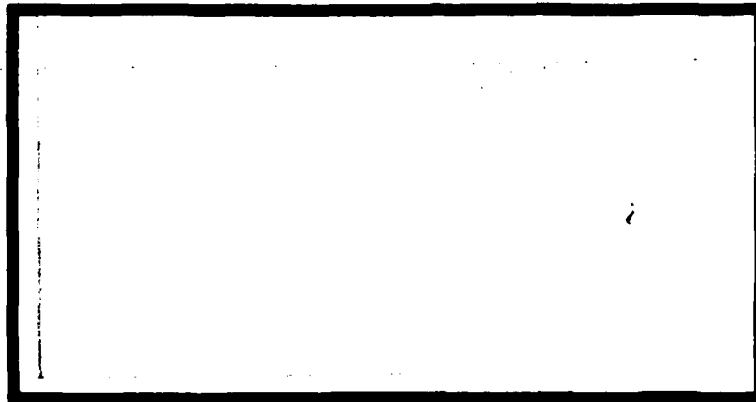


① LEVEL II  
D.S.



ADA 081 907

DTIC  
ELECTE  
MAR 18 1980  
S B D



UNITED STATES AIR FORCE  
AIR UNIVERSITY  
AIR FORCE INSTITUTE OF TECHNOLOGY  
Wright-Patterson Air Force Base, Ohio

DTIC FILE COPY

**DISTRIBUTION STATEMENT A**  
Approved for public release;  
Distribution Unlimited

80 3 14 027

① LEVEL II

AFIT/GAE/AA/78D-11

SLIP DAMPING  
OF  
TURBINE BLADES

THESIS

AFIT/GAE/AA/78D-11<sup>v</sup>

Michael C. Kimberling  
Capt USAF

DTIC  
ELECTE  
MAR 18 1980  
S D

B

**DISTRIBUTION STATEMENT A**

Approved for public release;  
Distribution Unlimited

AFIT/GAE/AA/78D-11

SLIP DAMPING  
OF  
TURBINE BLADES.

THESIS

Presented to the Faculty of the School of Engineering ✓  
of the Air Force Institute of Technology  
Air Training Command  
in Partial Fulfillment of the  
Requirements for the Degree of  
Master of Science

by

Michael C. Kimberling, B.S.

Capt

USAF

Graduate Engineering Aeronautics

December 1978

Acknowledgements

I would like to take this opportunity to express my gratitude to some of those individuals who were most prominent in assisting me to complete this effort. My thesis advisor, Dr. Peter J. Torvik, who assisted me in understanding many aspects of this study, and Dr. Clarence Edstrom, who assisted me with much of the mathematical work done for this study, are both deserving of recognition for their efforts. The same must be said for Captain Dan Hayes who was invaluable in helping me with the experimental portion of this study. Also worthy of note was the excellent support provided by the AFIT shops in the manufacturing of the experimental model.

ACCESSION for	
NTIS	White Section <input checked="" type="checkbox"/>
DOC	Buff Section <input type="checkbox"/>
UNANNOUNCED	<input type="checkbox"/>
JUSTIFICATION _____	
BY _____	
DISTRIBUTION/AVAILABILITY CODES	
Dist. AVAIL. and/or SPECIAL	
A	

Contents

	Page
Acknowledgements . . . . .	ii
List of Figures . . . . .	v
List of Tables . . . . .	vi
List of Symbols . . . . .	vii
Abstract . . . . .	ix
I. Introduction . . . . .	1
II. Experimental Development . . . . .	3
Model Description . . . . .	3
Test Set-up . . . . .	8
Test Procedure . . . . .	8
Data and Discussion . . . . .	11
III. Analytical Development . . . . .	18
Model Description . . . . .	18
Contact Surface State of Stress . . . . .	18
Contact Surface Displacements . . . . .	23
Points of Slip Initiation, and Zero Normal Force . . . . .	31
Energy Dissipated by Slip . . . . .	33
Energy Dissipated by Air Damping . . . . .	33
Energy Dissipated by Hysteresis . . . . .	34
Restoring Moment Due to Slip . . . . .	35
Equation of Motion and Boundary Conditions . . . . .	36
Solution to Equation of Motion . . . . .	37
IV. Recommendations . . . . .	44
Bibliography . . . . .	45

	Page
Appendix A: Eigenvalues and Corresponding Frequencies for Characteristic Equation . . . . .	47
Appendix B: Accelerometer and Impedance Head Calibration . .	49
Appendix C: Spring Beam Calibration . . . . .	51
Vita . . . . .	53

List of Figures

Figure		Page
1	Picture of Experimental Blade Model . . . . .	4
2	Dimensions and Sign Convention of Both Models . . . . .	5
3	Picture of Experimental Disk Model . . . . .	4
4	Picture of Assembled Disk-Blade Model (side view) . . . . .	6
5	Picture of Assembled Disk-Blade Model (end view) . . . . .	6
6	Picture of Spring Beam . . . . .	7
7	Schematic of Test Set-up . . . . .	9
8	Picture of Test Set-up in Lab . . . . .	10
9	Plot of Force Versus Frequency for $P = 10$ lbs and Variations in Tip Displacement . . . . .	12
10	Plot of Force Versus Frequency for $P = 20$ lbs and Variations in Tip Displacement . . . . .	14
11	Plot of Force Versus Frequency for Displacement = .0001 in. and Variations in $P$ . . . . .	16
12	Plot of Force Versus Frequency for Displacement = .0003 in. and Variations in $P$ . . . . .	17
13	Breakdown of Applied Loads . . . . .	19
14	Typical Stress Distribution of Contact Surface . . . . .	24
15	Relative Displacement Across Contact Region . . . . .	30
16	Schematic of Calibration Set-up for the Accelerometer and Impedance Head Calibration . . . . .	50
17	Picture of Force Table and Guide . . . . .	52
18	Picture of Force Table in Place on the Disk Model . . . . .	52

List of Tables

Table	Page
1 Listing of Eigenvalues and Natural Frequencies For the Homogeneous Beam . . . . .	48

### List of Symbols

P	Force applied by setscrew and spring beam (lbf)
$\theta_1$	Angle defining the contact surface of the disk model
L	Length of blade (in)
F	Magnitude of sinusoidal blade tip force (lbf)
r	Radius of blade root (in)
t	Depth of blade root (in)
b	Width of blade model (in)
$\phi_1, \phi_2, \phi_3$	Stress functions
Q,R	Points of slip initiation on contact surface (deg)
$\sigma_r$	Radial stress (lb/in <sup>2</sup> )
$\sigma_\theta$	Tangential stress (lb/in <sup>2</sup> )
$\tau_{r\theta}$	Shear stress (lb/in <sup>2</sup> )
M	Restoring moment due to slip (in-lb)
$\mu_D$	Dynamic coefficient of friction
$\mu_S$	Static coefficient of friction
$\delta T$	Variation in kinetic energy of blade
$\delta U$	Variation in potential energy of blade
$\delta WK$	Variation in work
$\gamma$	Mass per unit length of blade (lbm/in)
$I_o$	Mass moment of inertia of blade root about point O (lbm-in <sup>2</sup> )
W(X,T)	Displacement of the blade in the y direction
E	Modulus of elasticity of the blade (386lbm/sec <sup>2</sup> in)
I	Area moment of inertia of the blade (in <sup>4</sup> )
$\omega, \psi^2$	Forcing frequency
$\hat{\omega}$	Natural frequency of system
$\nu$	Poisson's Ratio

$D_o$	Energy dissipated per loading cycle (in-lbs)
U	Radial component of displacement
V	$\theta$ component of displacement
G	Modulus of rigidity
$\rho$	Mass density of air (slugs/ft <sup>3</sup> )
S	Wetted area of blade
$C_D$	Drag Coefficient

Abstract

An experimental, and an analytical, model of Turbine/Compressor blade with a circular root geometry is developed for the purpose of studying the effects of slip damping on the response of the blade. The expression for the energy dissipated by slip damping is presented. In addition the expressions for the energy dissipated by air and hysteresis damping are presented. The equation of motion for the blade is developed, and solved, to provide an expression relating the various parameters of the experimental and analytical models.

## I. Introduction

Today there are significant problems associated with the failure of Turbine/Compressor blades. The failures are due to increasing demands in the areas of performance and service life from the jet engines. To increase the performance, higher thrust to weight ratios are demanded. As a result, the excess material of the Turbine/Compressor blades is being reduced to the absolute minimum and the margins of safety are being reduced to the minimum allowable limits. Longer service life requirements have brought about problems with fatigue which are difficult to predict due to the random nature of the dynamic loading.

The environment of the Turbine/Compressor blade is very severe. The stresses generated within the Turbine/Compressor blades are very high. The loading which acts on the blades is very dynamic and random. The loading is especially severe at the resonant frequencies of the Turbine/Compressor blades where there is increased displacement which results in an increase in the stresses. In addition, for Turbine blades, there is the additional problem of a very high temperature environment.

It is important to understand the mechanisms which operate to reduce the effect of this dynamic loading. With a knowledge of these damping mechanisms, it might be possible to exploit them to obtain a further reduction in the effect of the dynamic loading.

There are three damping mechanisms which operate to reduce the response of a Turbine/Compressor blade. They are hysteresis or material damping, air damping, and slip damping. This paper is concerned with slip damping and so the other two forms of damping were addressed only to the degree necessary to provide the means of isolating the effect of the slip damping.

This study was undertaken to establish both an experimental, and an analytical model of a Turbine/Compressor blade. These models may be used to study the effect of slip damping on the response of a system similar to a Turbine/Compressor blade mounted in a disk. The analytical and experimental models might also be used to study ways of increasing the slip damping which occurs on the contact surface between the blade root and the disk. For example, if the slip damping mechanism could be maintained at higher engine RPM levels there would be a significant contribution to the reduction of the response of the Turbine/Compressor blade.

The primary area of investigation presented in this paper is the development of the analytical model. All equations and relationships required to predict the response of the Turbine/Compressor blade to a specified loading condition were compiled. In addition, the equations required to predict the amount of energy dissipated per cycle by the three forms of damping were developed. The experimental model was used to generate data for several variations in loading conditions for the purpose of validating the model for use as a tool for the experimental study of slip damping.

## II. Experimental Development

### Model Description

Figure 1 is a picture of the experimental blade model. A uniform beam with a half cylinder fixed to one end was chosen as a simplified model of a turbine or compressor blade. Due to the limitations of this investigation, and the phenomenon being studied, this simplification was felt to be acceptable. The half cylinder is the root for the experimental blade model. The shape was chosen to facilitate both the manufacturing of the model and the analytical work. The dimensions of the experimental model are shown in Figure 2. Figure 3 is a picture of the experimental disk model. The assembled blade-disk model (Figures 4 and 5) provides a simple representation of a turbine or compressor blade mounted in an engine disk. In a jet engine the primary force acting on the blade root is due to the inertia load of the blade on the blade root which is produced by the disk and blade rotating during engine operation. To simulate this loading, in the blade-disk model, a spring beam with a pointed screw was used to apply a point load to the blade root at the point of rotation for the blade root (Figure 6). The beam was instrumented on both sides at a chosen point with strain gages to allow for the determination of the clamping force. The blade-disk model was manufactured using Inconel-X. This material was chosen because it is representative of the materials used in a jet engine and to allow the use of the blade-disk model at elevated temperatures without severe changes in the material properties. The properties for Inconel-X are:

$$\text{Modulus of elasticity (E)} = 31 \times 10^6 \text{ lbf/in}^2$$

$$\text{Poisson's ratio (v)} = .29$$

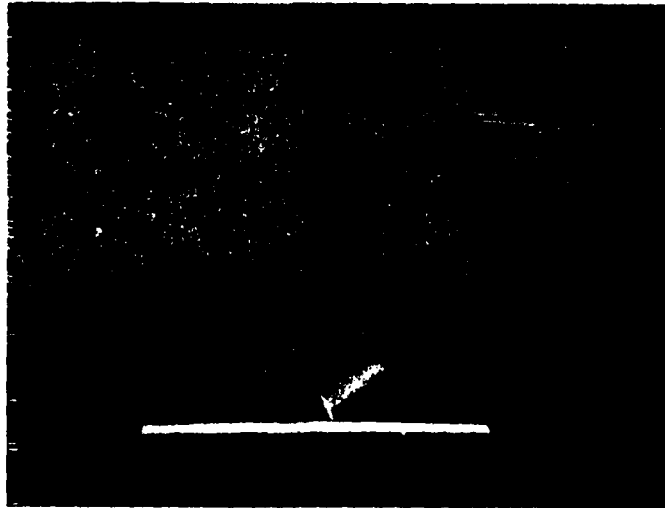


Figure 1. Picture of Experimental Blade Model

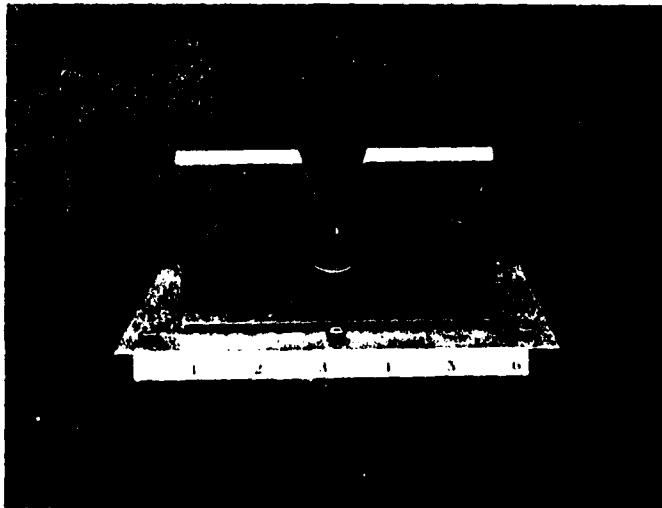


Figure 3. Picture of Experimental Disk Model

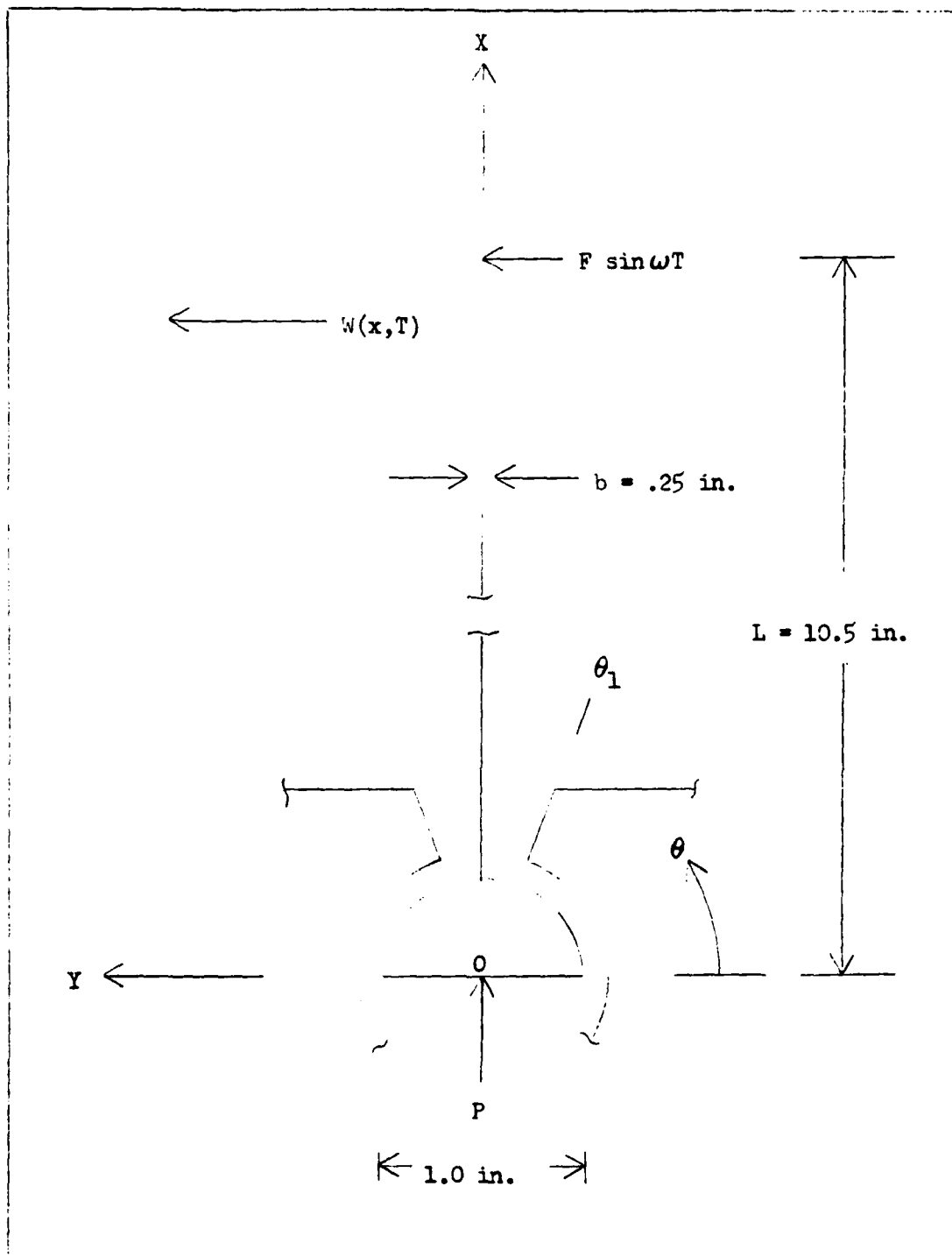


Figure 2. Dimensions and Sign Convention of Both Models

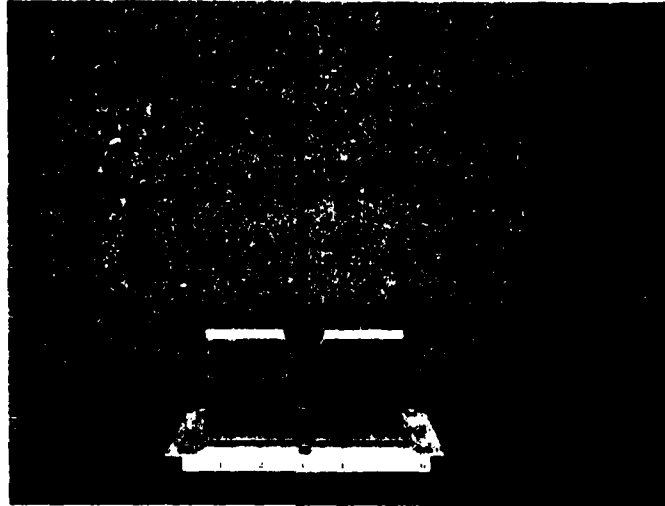


Figure 4. Picture of Assembled Disk-Blade Model  
(side view)

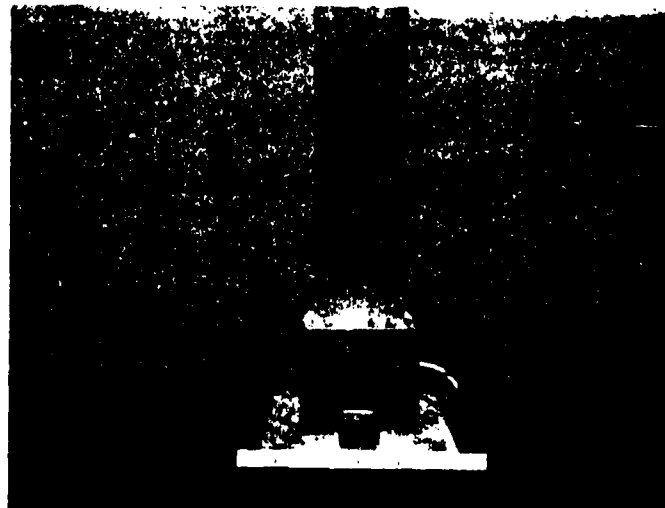


Figure 5. Picture of Assembled Disk-Blade Model  
(end view)

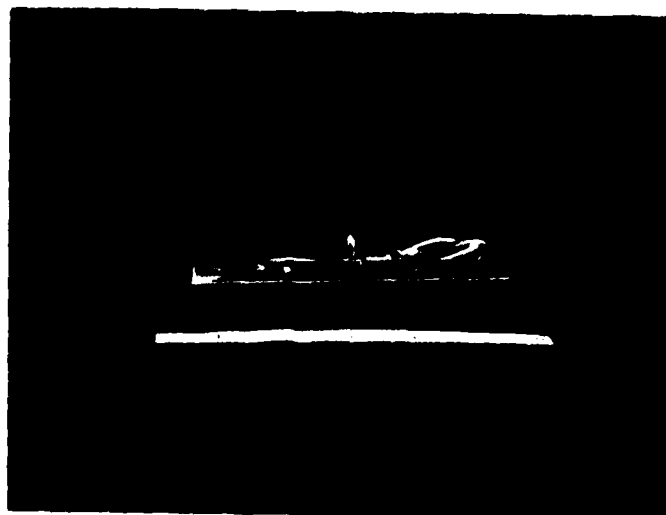


Figure 6. Picture of Spring Beam

Static coefficient of friction ( $\mu_s$ ) = 1.1

Dynamic coefficient of friction ( $\mu_d$ ) = .5

#### Test Set-up

Figure 7 is a schematic diagram of the test set-up which is pictured in Figure 8. A MB model N695 Automatic Vibration Exciter Controller was used to adjust the frequency and the magnitude of the signal being fed thru the MB model 2120MB Amplifier to the MB model EA1500 Exciter. The exciter applied a sinusoidal force to the tip of the blade to simulate the dynamic loading of a compressor or turbine blade which occurs in a jet engine. The magnitude of the applied force was monitored using a Wilcoxon model Z11 impedance head. The force gage signal from the impedance head was amplified using a Kistler model 568 charge amplifier and displayed on a Tektronix model 465M dual trace oscilloscope. Due to problems with the integral accelerometer within the impedance head, a separate accelerometer, mounted on the blade tip, was used to measure blade tip displacement. The signal from the MB model 306 accelerometer was amplified using a Kistler model 504D charge amplifier and displayed on the same scope as the force gage signal. The signal from the strain gages was monitored using a Tektronix type 549 oscilloscope with a plug-in dynamic strain preamplifier.

#### Test Procedure

Due to the nature of the test set-up, with the blade tip constrained by the physical attachment of the exciter, it was not possible to study the displacement of the blade tip to a known force at resonance. Instead the force required to maintain a set displacement at resonance was monitored. The procedure for collecting the data was:

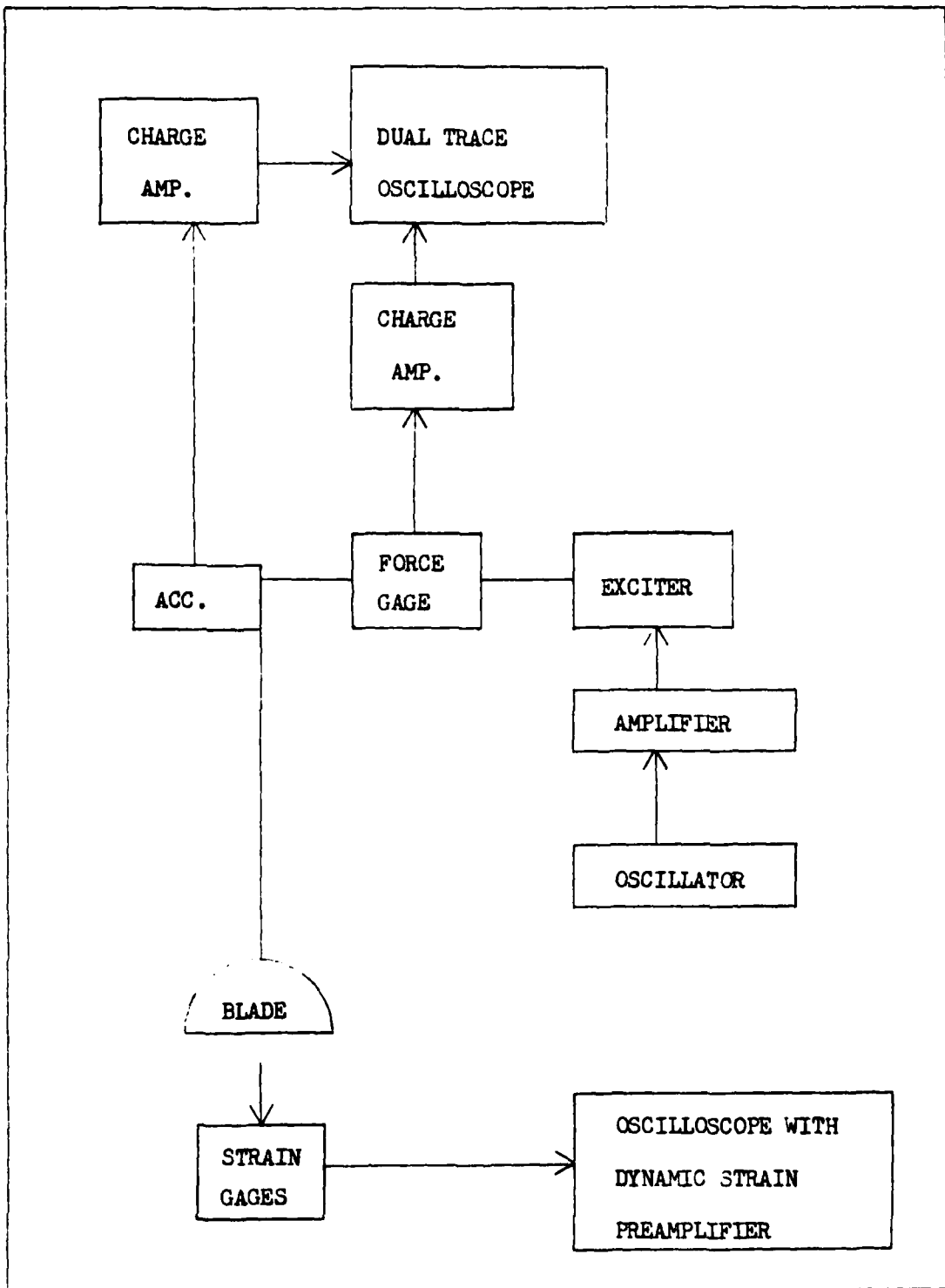


Figure 7. Schematic of Test Set-up

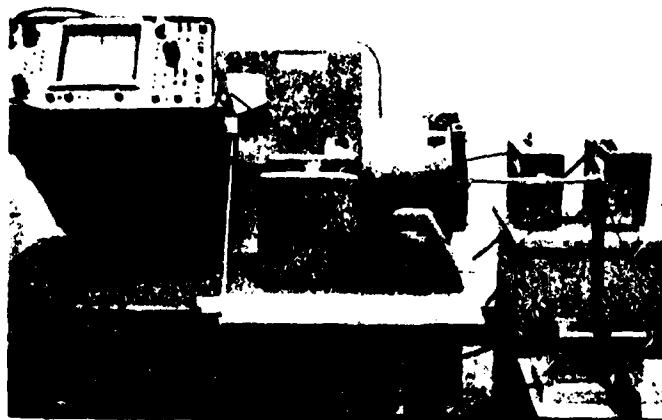


Figure 8. Picture of Test Set-up in Lab

1) The force gage and the accelerometer were calibrated using the procedure outlined in Appendix B.

2) The spring beam strain gages were calibrated using the procedure of Appendix C.

3) A force was applied to the blade root using the set screw and spring beam.

4) A displacement for a data run was selected.

5) A frequency was selected for a data point within the data run.

6) Using:  $\text{displacement} = \text{acceleration} / (2\pi \text{ frequency})^2$

the acceleration required for the desired displacement at the selected frequency was determined.

7) Using the controller/oscillator, the needed acceleration was set.

8) The magnitude of the force being exerted to maintain the displacement was recorded.

9) A new frequency was selected and steps 6, 7, and 8 were repeated. This was done at as many data points within a set displacement data run as desired.

10) Steps 4 thru 9 were repeated for different values of the clamping pressure.

Since the frequency range of interest was the range about a point of resonance, the frequency range for the data runs was selected about the first resonant frequency calculated which was calculated in Appendix A.

#### Data and Discussion

Figure 9 is a plot of the force versus frequency for a clamping pressure of ten pounds and three variations in the value of blade tip displacement. The first item to note is the presence of the resonance at 320 cps. This corresponds almost exactly to the value of resonance which

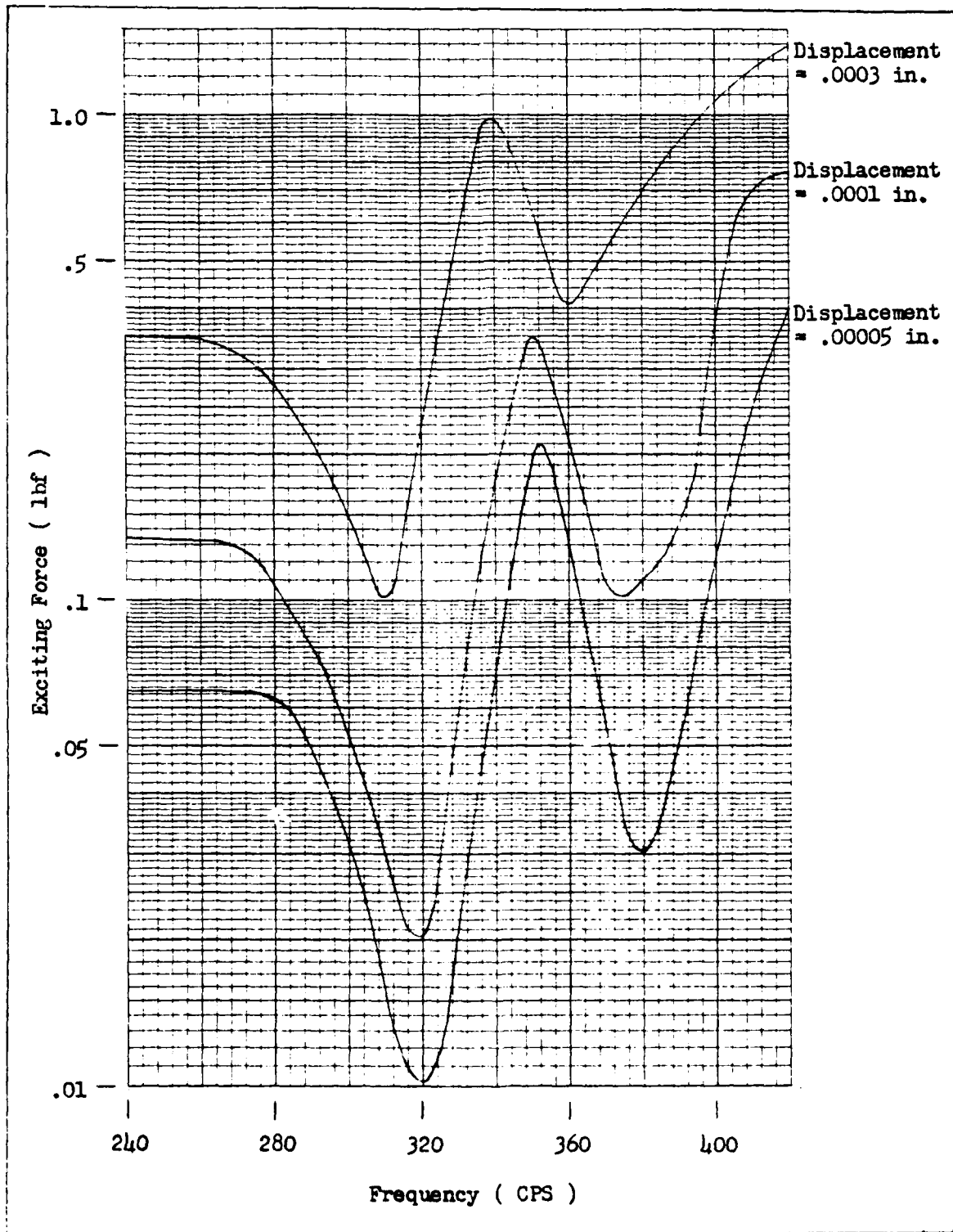


Figure 9. Plot of Force Versus Frequency for  $P = 10$  lbs and Variations in Tip Displacement

was predicted by the analytical model for the first mode of the blade. All data runs were made over the range of 240 to 420 cps, but a sweep was made to a frequency of 1200 cps to check for other possible resonances. This sweep verified the existence of a resonance at 1000 cps, within five per cent of the value of resonance which was predicted by the analytical model for the second mode of the blade.

With an increase in the blade tip displacement there is an increase in the magnitude of the blade tip driving force, for the displacements of .00005 in. and 0001 in. Figure 9 shows an amplification factor of 1 to 6.5 at 320 cps. This indicates no change in the damping of the system. This is difficult to understand in light of the fact that all the damping mechanisms are functions of the exciting force. The slip damping, however, will not be present until the exciting force reaches a threshold value. The third displacement data point of .0003 in. plotted in Figure 9 shows an amplification factor of 1 to 3.5 at 320 cps. This indicates a significant increase in the amount of damping, present in the system, at resonance. It may be assumed that the threshold value for slip damping has been passed and that slip damping is making a large contribution to the damping of the system.

Figure 10 is a plot of the force versus frequency for a clamping pressure of twenty pounds and three variations in the blade tip displacement. The analytically predicted resonance at 320 cps is present in this set of data. The amplification factors, for the resonance peak at 320 cps, for the lower two displacement cases are almost identical. The amplification factor for the largest displacement case shows a significant increase in the amount of damping present at resonance. Again it can be assumed that the critical value of the exciting force has been passed and

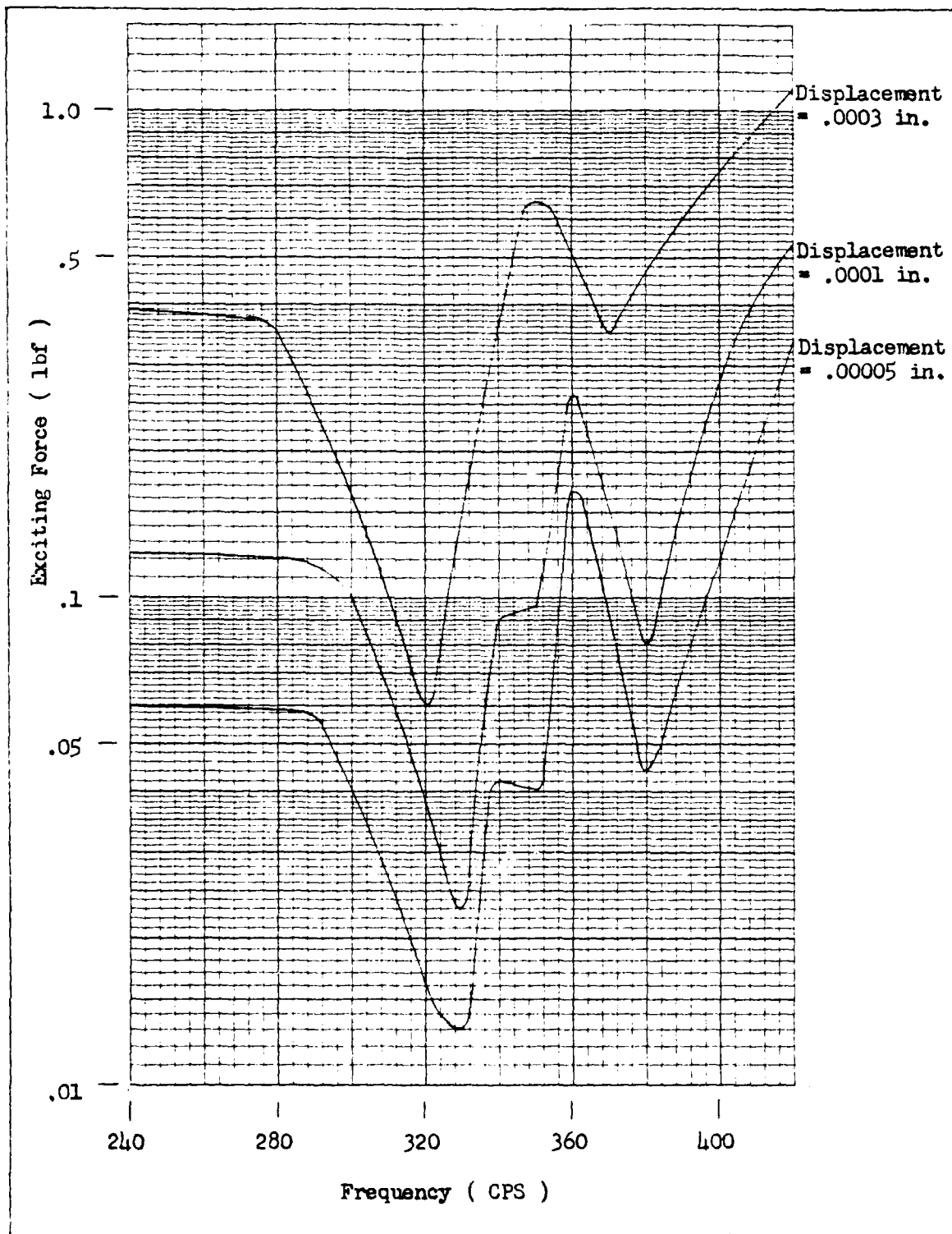


Figure 10. Plot of Force Versus Frequency for  $P = 20$  lbs and Variations in Tip Displacement

that slip damping is contributing to the dissipation of energy of the system.

Figures 11 and 12 are force versus frequency plots for a set displacement and variations in the clamping force. From these plots it can be seen that, for a set displacement, or exciting force, that the lower clamping pressure provides a better reduction of the amplification factor. This supports the conclusion that the lower the clamping pressure, the more slip damping is present. The exception to this occurs at 320 cps on Figure 11. The resonant amplification factors are almost identical. This can be explained by supposing that the particular value of the ratio of exciting force to clamping pressure is not high enough for slip to occur. The prominent resonance at 370 cps appears to correspond to the second torsional mode of the blade.

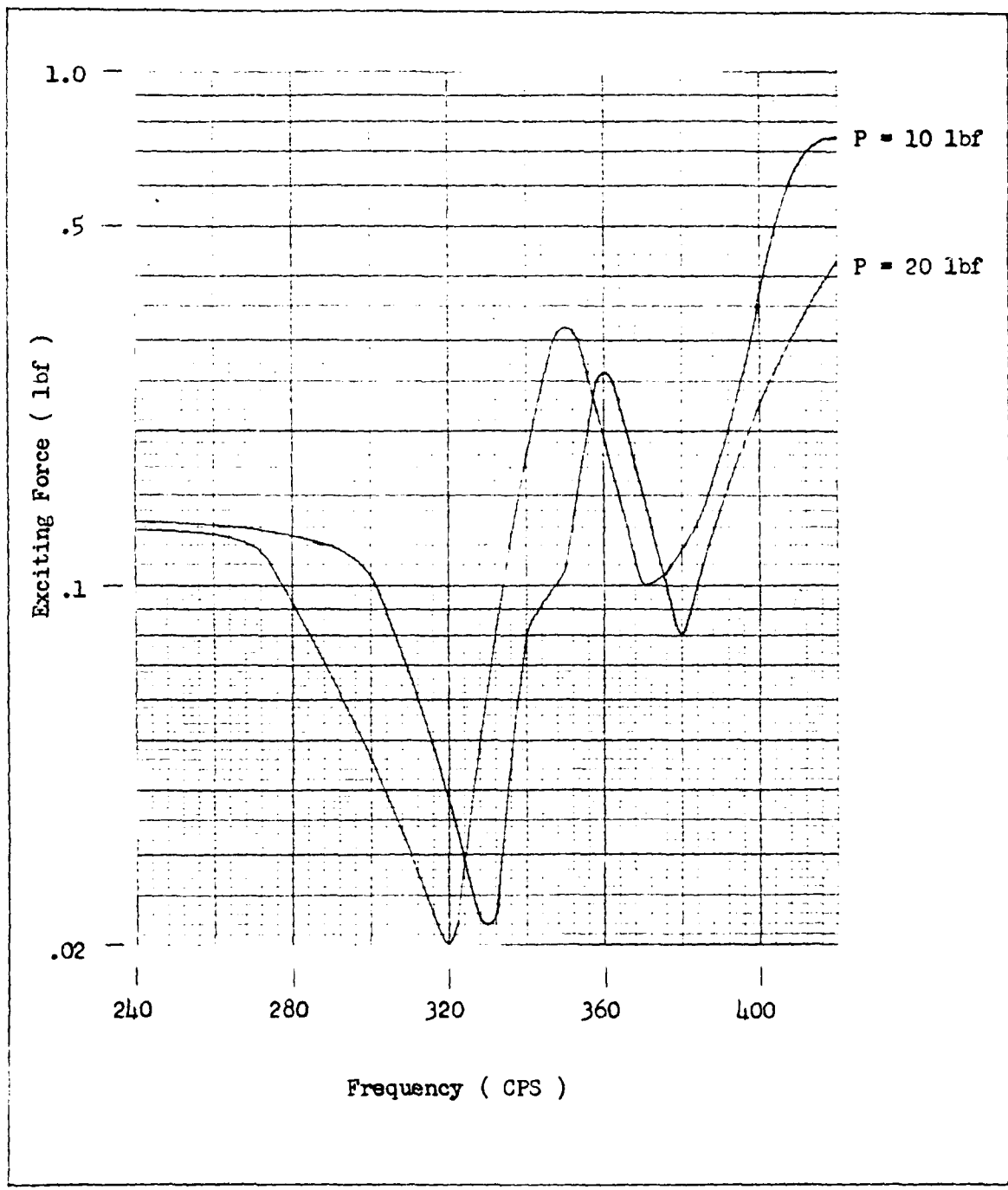


Figure 11. Plot of Force Versus Frequency for Displacement = .0001 in. and Variations in P

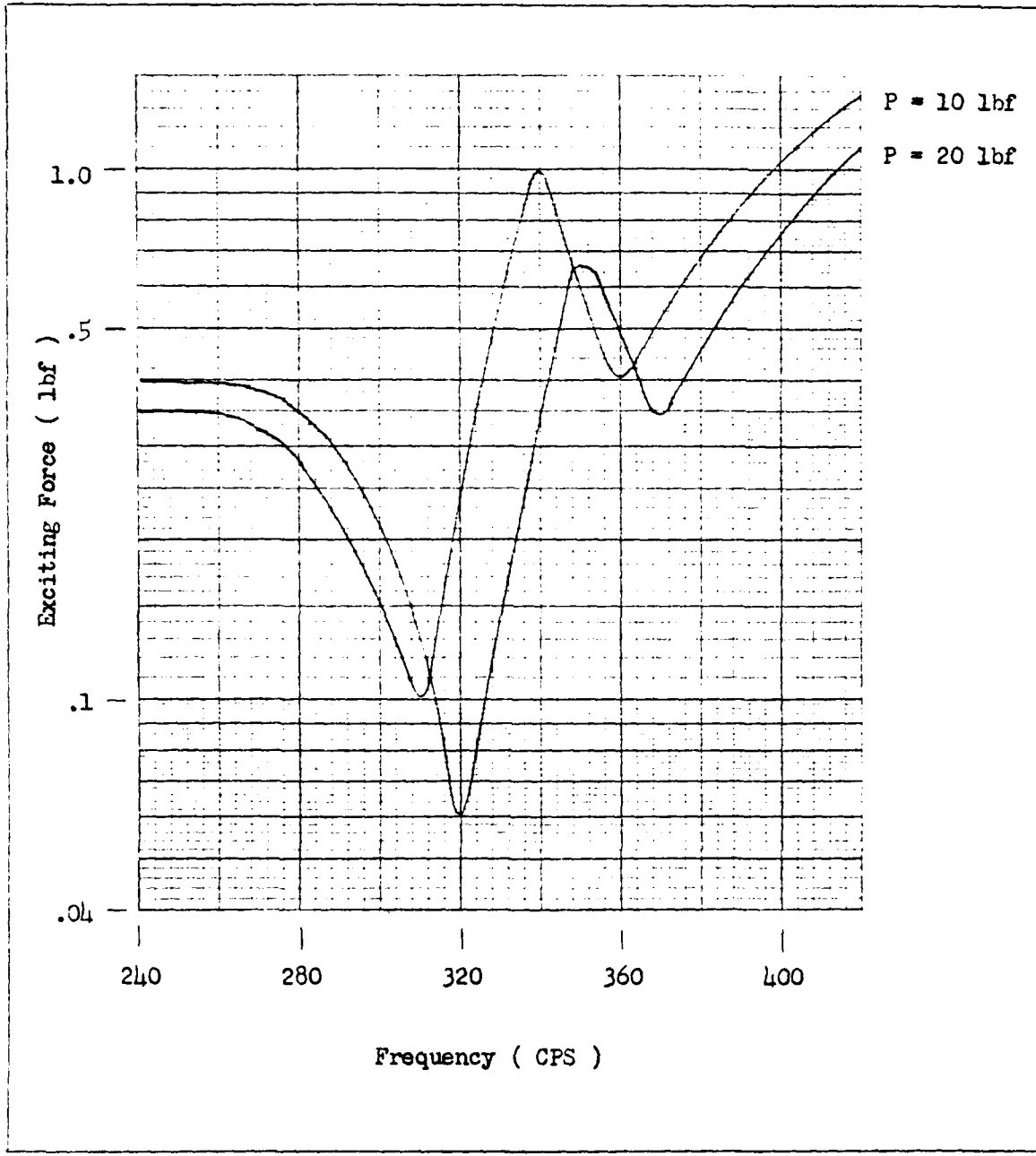


Figure 12. Plot of Force Versus Frequency for Displacement = .0003 in. and Variations in P

### III. Analytical Development

#### Model Description

Figure 2 shows the dimensions and sign convention of the analytical blade model that was used in this study. The blade was represented as a continuous beam of constant mass per unit length and constant cross sectional area.

#### Contact Surface State of Stress

The first step toward the calculation of the energy dissipated by slip is the calculation of the stresses acting on the contact surface. To determine the traction distribution on the blade contact surface required to maintain equilibrium, the loading on the blade root was broken into three cases (see Figure 13). Case one is the force applied to the bottom of the blade root by the setscrew. This force was intended to simulate the inertia force of a blade which acts on a turbine/compressor blade root due to the rotating motion of the blade-disk structure. Cases two and three are the transverse force and moment, respectively, which are applied to the blade root due to the dynamic force applied to the blade tip. The first two loading conditions were analyzed using the solutions for the stresses on a wedge loaded at it's apex. The half disk geometry of the model blade root can be matched by expanding the half angle of the wedge to 90 degrees. For the third loading case the solution for a disk loaded by a couple was used. By starting with the stress functions, for the wedge and disk solutions, and evaluating the constants based on the conditions of the blade root model, a good approximation of the stress condition of the contact surface can be obtained. Timoshenko (23) discusses the wedge and disk problems in great detail.

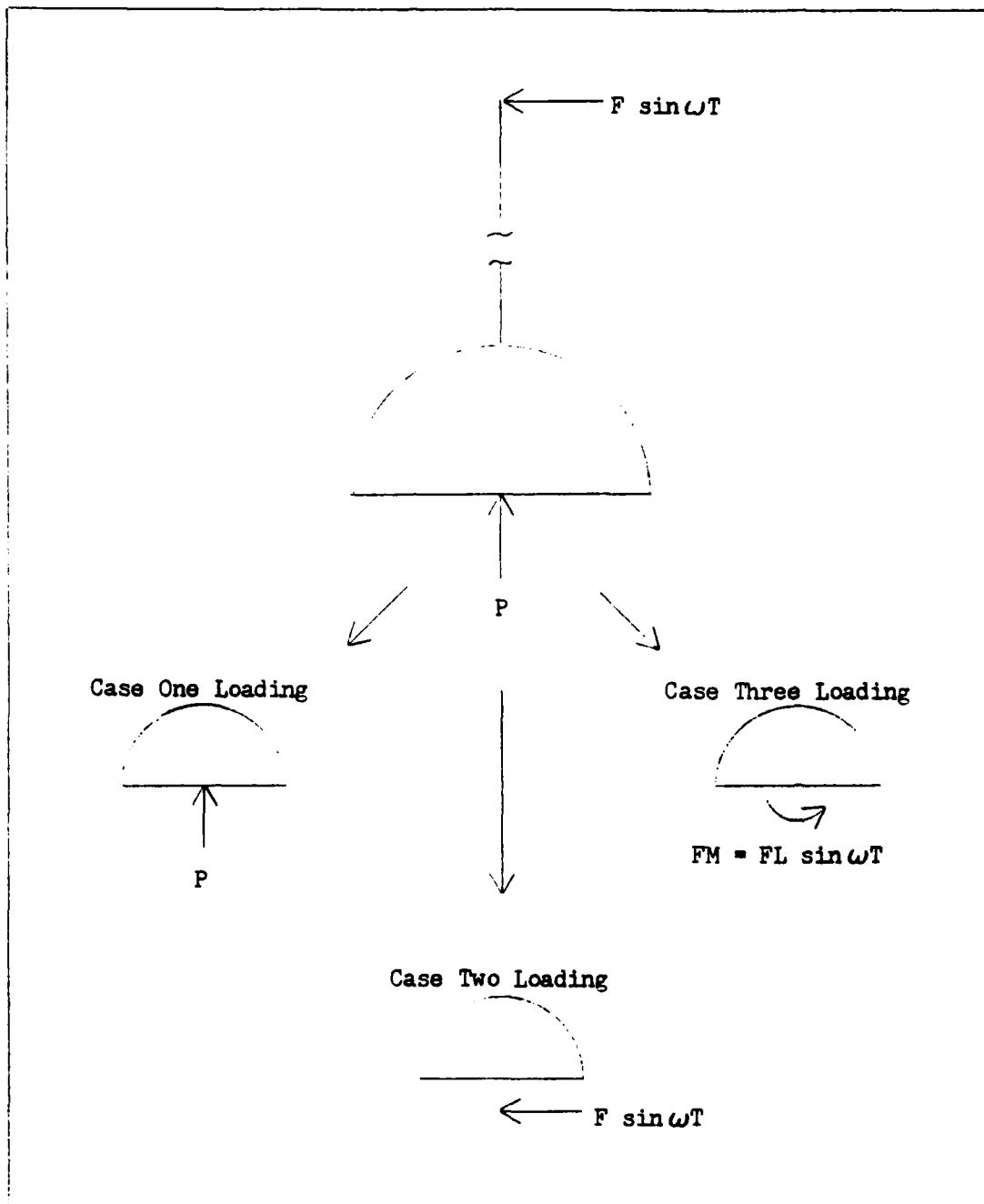


Figure 13. Breakdown of Applied Loads

1. Case One Loading

Using as the stress function

$$\phi_1 = A_1 r \theta \cos \theta \quad (1)$$

the following stresses were derived.

$$\sigma_r = -\frac{2}{r} A_1 \sin \theta \quad (2)$$

$$\sigma_\theta = \tau_{r\theta} = 0$$

To evaluate the constant  $A_1$ , the integral of the vertical component of stress over the contact surface was set equal to the applied force (P).

$$\int_0^t \left[ \int_0^{\theta_1} \sigma_r r \sin \theta d\theta + \int_{\pi-\theta_1}^{\pi} \sigma_r r \sin \theta d\theta \right] dz = -P \quad (3)$$

Substituting equations (2) into (3) and evaluating,

$$2A_1 \int_0^t \left[ \left( \frac{1}{2}\theta - \frac{1}{4}\sin 2\theta \right) \Big|_0^{\theta_1} + \left( \frac{1}{2}\theta - \frac{1}{4}\sin 2\theta \right) \Big|_{\pi-\theta_1}^{\pi} \right] dz = P \quad (4)$$

results in an expression for  $A_1$ .

$$A_1 = \frac{P}{t(2\theta_1 - \sin 2\theta_1)} \quad (5)$$

Using the above gives the stresses on the contact surface due to case one loading.

$$\sigma_r = \frac{2P \sin \theta}{rt(\sin 2\theta_1 - 2\theta_1)} \quad (6)$$

$$\sigma_\theta = \tau_{r\theta} = 0$$

2. Case Two Loading

Using as the stress function,

$$\phi_2 = A_2 r \theta \sin \theta \quad (7)$$

the following stresses were derived.

$$\sigma_{\theta} = \tau_{r\theta} = 0 \quad (8)$$

$$\sigma_r = \frac{2}{r} A_2 \cos\theta$$

To evaluate the constant  $A_2$ , the integral of the horizontal component of stress over the contact surface was set equal to the applied force ( $F \sin\omega T$ ).

$$\int_0^t \left[ \int_0^{\theta_1} \sigma_r r \cos\theta d\theta + \int_{\pi-\theta_1}^{\pi} \sigma_r r \cos\theta d\theta \right] dz = -F \sin\omega T \quad (9)$$

results in an expression for  $A_2$ .

$$A_2 = \frac{F \sin\omega T}{t(2\theta_1 + \sin 2\theta_1)} \quad (10)$$

Using the above gives the stresses on the contact surface due to case two loading.

$$\sigma_r = \frac{2F \sin\omega T \cos\theta}{rt(2\theta_1 + \sin 2\theta_1)} \quad (11)$$

$$\sigma_{\theta} = \tau_{r\theta} = 0$$

### 3. Case Three Loading

Using as the stress function,

$$\phi_3 = A_3 \theta \quad (12)$$

the following stresses were derived.

$$\sigma_r = \sigma_{\theta} = 0 \quad (13)$$

$$\tau_{r\theta} = \frac{A_3}{r^2}$$

Solving for  $A_3$  by setting the integral of the shear over the area of the contact surface equal to the moment caused by the blade tip load ( $FL \sin\omega T = FM$ ).

$$FM + \int_0^t \left[ \int_0^{\theta_1} \tau_{r\theta} r^2 d\theta + \int_{\pi-\theta_1}^{\pi} \tau_{r\theta} r^2 d\theta \right] dz = 0 \quad (14)$$

Substituting equations (13) into (14) and evaluating,

$$-FM = \int_0^t A_3 \left[ \theta \Big|_0^{\theta_1} + \theta \Big|_{\pi-\theta_1}^{\pi} \right] dz \quad (15)$$

results in an expression for  $A_3$ .

$$A_3 = \frac{-FM}{2t\theta_1} \quad (16)$$

Putting equation (16) into equations (13) gives the stresses due to case three loading.

$$\begin{aligned} \sigma_r = \sigma_\theta &= 0 \\ \tau_{r\theta} &= \frac{-FM}{2r^2\theta_1 t} \end{aligned} \quad (17)$$

The results from the three separate loading conditions can be combined, using the principle of superposition, to provide an expression for the total stress condition of the contact surface.

$$\sigma_r = \frac{2P \sin\theta}{rt(\sin 2\theta_1 - 2\theta_1)} + \frac{2F \sin\omega T \cos\theta}{rt(2\theta_1 + \sin 2\theta_1)} \quad (18)$$

$$\tau_{r\theta} = \frac{-FM}{2r^2 t \theta_1} \quad (19)$$

$$\sigma_\theta = 0 \quad (20)$$

As the blade loading of the blade root increases, the shear stress on the contact surface of the blade root increases in magnitude. As the value of the shear stress at a point on the contact surface reaches a value equal to the friction force, opposing motion, slip will occur. The friction force is generated by the radial stress times the static

coefficient of friction. Slip will continue until the shear force, at the point, drops to a value which is less than the friction force caused by the radial stress times the dynamic coefficient of friction.

A non-dimensional representation of the stress distribution on the contact surface is pictured in Figure 14. The direction of the exciting force is also depicted in the figure. It can be seen from the figure that the normal force is not independent of the exciting force. The static and dynamic friction forces will always be negative while the shear force will change, from positive to negative, depending on the direction of the exciting force.

The energy dissipated by slip is the integral, over the slip region, of the friction force times the relative displacement across the contact surface. If the normal force was independent of the exciting force, then the relative displacement across the contact surface could be related to the change in the stress component, parallel to the contact surface, across the contact surface. Instead the relative displacement must be calculated by first solving for the displacements associated with the contact surface stresses.

#### Contact Surface Displacements

Associated with the three loading cases previously discussed are the displacements which occur at points on the contact surface. To solve for the displacements the equations for the relationships of stress to strain, and strain to displacement were used.

$$\epsilon_r = \frac{\partial U}{\partial r} = \frac{1}{E} (\sigma_r - \nu \sigma_\theta) \quad (21)$$

$$\epsilon_\theta = \frac{U}{r} + \frac{1}{r} \frac{\partial V}{\partial \theta} = \frac{1}{E} (\sigma_\theta - \nu \sigma_r) \quad (22)$$

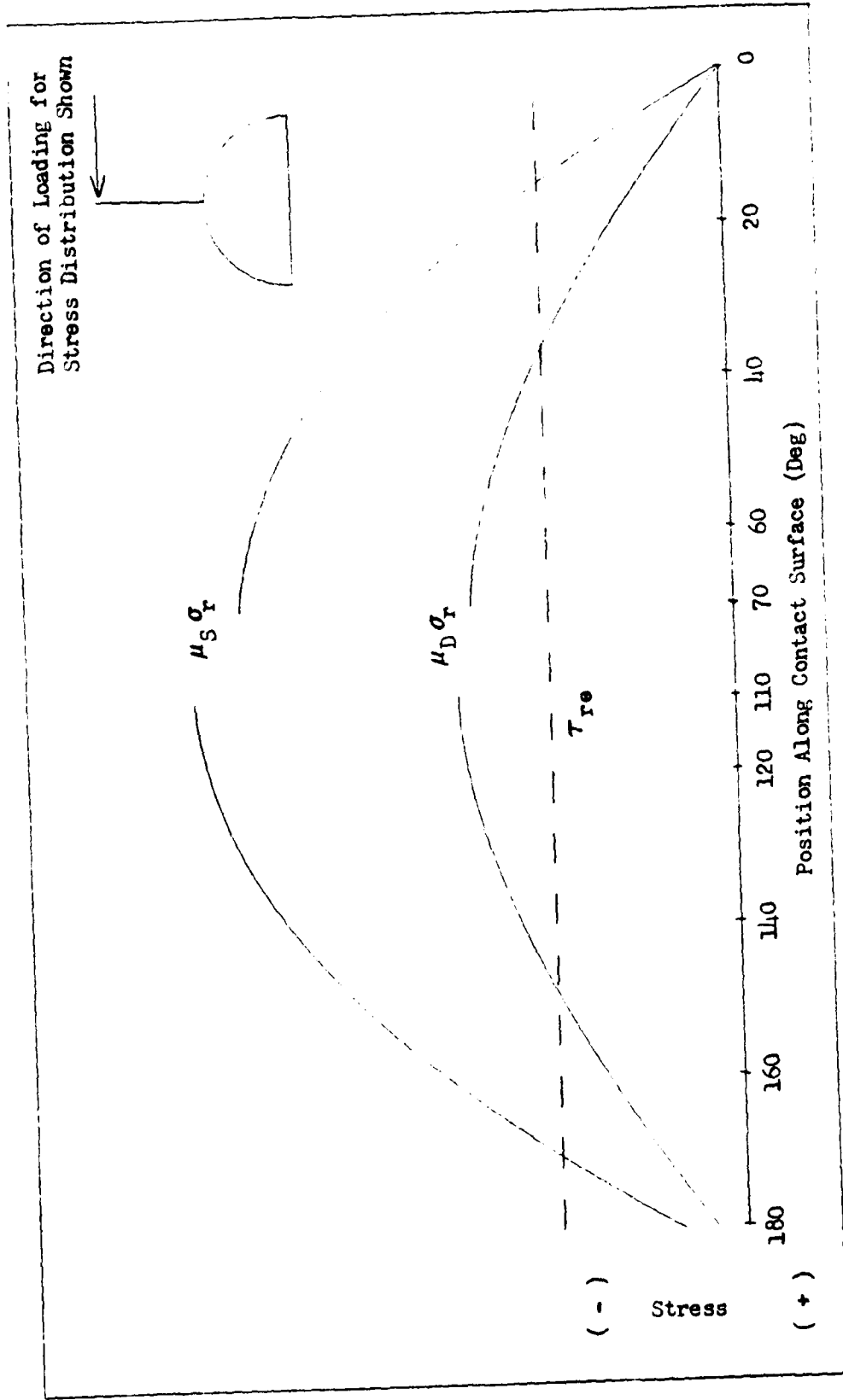


Figure 11. Typical Stress Distribution of Contact Surface

$$\epsilon_{r\theta} = \frac{1}{r} \frac{\partial U}{\partial \theta} + \frac{\partial V}{\partial r} - \frac{V}{r} = \frac{1}{G} \tau_{r\theta} \quad (23)$$

1. Case One Loading

Using equations (6) and equation (21) the U displacement is

$$U = - \frac{2P \sin \theta \log r}{tE(2\theta_1 - \sin 2\theta_1)} + f(\theta) \quad (24)$$

Using equations (24) and (22) the V displacement can be solved for.

$$V = - \frac{2\nu P \cos \theta}{tE(2\theta_1 - \sin 2\theta_1)} - \frac{2P \cos \theta \log r}{tE(2\theta_1 - \sin 2\theta_1)} - \int f(\theta) d\theta + f(r) \quad (25)$$

To solve for  $f(\theta)$  and  $f(r)$ , equation (23) and equation (6) are used along with equations (24) and (25). Using these equations an expression in terms of  $f(\theta)$  and  $f(r)$  is developed.

$$\begin{aligned} \frac{\partial f(\theta)}{\partial \theta} \frac{1}{r} - \frac{2P \cos \theta}{rtE(2\theta_1 - \sin 2\theta_1)} + \frac{\partial f(r)}{\partial r} + \frac{2\nu P \cos \theta}{rtE(2\theta_1 - \sin 2\theta_1)} \\ + \int \frac{f(\theta)}{r} d\theta - \frac{f(r)}{r} = 0 \end{aligned} \quad (26)$$

For this equation to hold the sum of the  $\theta$  terms must be equal to zero and the sum of the  $r$  terms must be equal to zero. Timoshenko (23) discusses the solution to equation (26) for  $f(\theta)$  and  $f(r)$ .

$$f(r) = Q_1 r \quad (27)$$

and

$$f(\theta) = f(\text{particular}) + f(\text{homogeneous}) \quad (28)$$

The particular solution is dependent on the other  $\theta$  terms present in the expression for  $f(\theta)$  and  $f(r)$ , equation (26).

$$f(\theta) = - \frac{P(\nu - 1)\theta \cos \theta}{tE(2\theta_1 - \sin 2\theta_1)} + Q_2 \sin \theta + Q_3 \cos \theta \quad (29)$$

Using equations (27) and (28), the displacements are

$$U = - \frac{2P \sin \theta \log r}{tE(2\theta_1 - \sin 2\theta_1)} - \frac{P(\nu - 1)\theta \cos \theta}{tE(2\theta_1 - \sin 2\theta_1)} + Q_2 \sin \theta + Q_3 \cos \theta \quad (30)$$

and

$$V = -\frac{2\nu P \cos\theta}{tE(2\theta_1 - \sin 2\theta_1)} - \frac{2P \cos\theta \log r}{tE(2\theta_1 - \sin 2\theta_1)} + \frac{P(\nu - 1) \cos\theta}{tE(2\theta_1 - \sin 2\theta_1)} \\ + \frac{P(\nu - 1) \sin\theta}{tE(2\theta_1 - \sin 2\theta_1)} + Q_2 \cos\theta + Q_3 \sin\theta + Q_1 r \quad (31)$$

Selecting for a boundary condition that the displacements (U and V) are equal to zero at the point on the contact surface where  $\theta = 0$  allows the evaluation of the constants in equations (30) and (31).

$$Q_1 = 0$$

$$Q_2 = \frac{P(\nu + 1)}{tE(2\theta_1 - \sin 2\theta_1)} + \frac{2P \log r}{tE(2\theta_1 - \sin 2\theta_1)} \quad (32)$$

$$Q_3 = 0$$

Substituting equations (32) into equations (30) and (31)

$$U = -\frac{P(\nu - 1)\theta \cos\theta}{tE(2\theta_1 - \sin 2\theta_1)} + \frac{P(\nu + 1) \sin\theta}{tE(2\theta_1 - \sin 2\theta_1)} \quad (33)$$

and

$$V = \frac{P(\nu - 1)\theta \sin\theta}{tE(2\theta_1 - \sin 2\theta_1)} \quad (34)$$

## 2. Case Two Loading

Using equations (11) and equation (21) the U displacement is

$$U = \frac{2F \sin\omega T \cos\theta}{tE(2\theta_1 + \sin 2\theta_1)} \log r + f(\theta) \quad (35)$$

Using equations (35) and (22) the V displacement is

$$V = -\frac{2F \sin\omega T \sin\theta}{tE(2\theta_1 + \sin 2\theta_1)} \log r - \frac{2\nu F \sin\omega T \sin\theta}{tE(2\theta_1 + \sin 2\theta_1)} \\ - \int f(\theta) d\theta + f(r) \quad (36)$$

To solve for  $f(\theta)$  and  $f(r)$  the same method is employed as was used for the case one loading displacement analysis. The results are

$$f(r) = Q_1 r \quad (37)$$

and

$$f(\theta) = \frac{(\nu - 1) F \sin \omega T \cos \theta}{tE(2\theta_1 + \sin 2\theta_1)} + Q_2 \sin \theta + Q_3 \cos \theta \quad (38)$$

These results, when used with equations (35) and (36) provide the following displacement expressions,

$$U = \frac{2F \sin \omega T \log r \cos \theta}{tE(2\theta_1 + \sin 2\theta_1)} + \frac{(\nu - 1) F \sin \omega T \cos \theta}{tE(2\theta_1 + \sin 2\theta_1)} + Q_2 \sin \theta + Q_3 \cos \theta \quad (39)$$

and

$$V = \frac{2F \sin \omega T \log r \sin \theta}{tE(2\theta_1 + \sin 2\theta_1)} - \frac{(\nu - 1) F \sin \omega T \cos \theta}{tE(2\theta_1 + \sin 2\theta_1)} - \frac{(\nu - 1) F \sin \omega T \sin \theta}{tE(2\theta_1 + \sin 2\theta_1)} + Q_2 \cos \theta - Q_3 \sin \theta + Q_1 r \quad (40)$$

To solve for the constants in equations (39) and (40) the displacement at the point  $\theta = 0$  is set equal to zero. Using this boundary condition the constants are

$$Q_1 = 0$$

$$Q_2 = - \frac{(\nu - 1) F \sin \omega T}{tE(2\theta_1 + \sin 2\theta_1)} \quad (41)$$

$$Q_3 = - \frac{2F \sin \omega T \log r}{tE(2\theta_1 + \sin 2\theta_1)}$$

Introducing equations (41) into equations (39) and (40)

$$U = \frac{(\nu + 1) F \sin \omega T \cos \theta}{tE(2\theta_1 + \sin 2\theta_1)} - \frac{(\nu - 1) F \sin \omega T \sin \theta}{tE(2\theta_1 + \sin 2\theta_1)} \quad (42)$$

and

$$V = - \frac{2(\nu - 1) F \sin \omega T \cos \theta}{tE(2\theta_1 + \sin 2\theta_1)} - \frac{(\nu - 1) F \sin \omega T \sin \theta}{tE(2\theta_1 + \sin 2\theta_1)} \quad (43)$$

### 3. Case Three Loading

Using equations (17) and equations (21) and (22) it is possible to establish the relationships

$$U = f(\theta) \quad (44)$$

and

$$v = - \int f(\theta) d\theta \quad (45)$$

Using equation (23) it is possible to set up an expression in terms of  $f(\theta)$

$$- \frac{FM}{2G r t \theta_1} = \frac{\partial f(\theta)}{\partial \theta} + \int f(\theta) d\theta \quad (46)$$

which can be solved for  $f(\theta)$

$$f(\theta) = Q_2 \sin\theta + Q_3 \cos\theta - \frac{FM}{2G r t \theta_1} \quad (47)$$

where

$$G = \frac{E}{2(1 + \nu)} \quad (48)$$

which gives the following displacements

$$U = Q_2 \sin\theta + Q_3 \cos\theta - \frac{FM}{2G r t \theta_1} \quad (49)$$

and

$$V = Q_2 \cos\theta - Q_3 \sin\theta + \frac{FM}{2G r t \theta_1} \quad (50)$$

The displacement at  $\theta = 0$  is set equal to zero in order to solve for the unknown constants. Solving for the constants  $Q_2$  and  $Q_3$  and putting them into equations (49) and (50) gives the final displacement equations

$$U = \frac{(1 + \nu) FM}{E r t \theta_1} (\cos\theta - 1) \quad (51)$$

and

$$V = \frac{(1 + \nu) FM}{E r t \theta_1} (\theta - \sin\theta) \quad (52)$$

The total displacements can be arrived at, in the same manner as the total stress components were achieved, by the principle of

superposition.

$$U = - \frac{P(\nu - 1)\theta \cos\theta}{tE(2\theta_1 - \sin 2\theta_1)} + \frac{P(\nu + 1) \sin\theta}{tE(2\theta_1 - \sin 2\theta_1)} + \frac{(\nu + 1) F \sin\omega T\theta \cos\theta}{tE(2\theta_1 + \sin 2\theta_1)} - \frac{(\nu - 1) F \sin\omega T \sin\theta}{tE(2\theta_1 + \sin 2\theta_1)} + \frac{(1 + \nu) FM (\cos\theta - 1)}{E r t \theta_1} \quad (53)$$

and

$$V = \frac{P(\nu - 1)\theta \sin\theta}{tE(2\theta_1 - \sin 2\theta_1)} - \frac{2(\nu - 1) F \sin\omega T \cos\theta}{tE(2\theta_1 + \sin 2\theta_1)} - \frac{(\nu - 1) F \sin\omega T\theta \sin\theta}{tE(2\theta_1 + \sin 2\theta_1)} + \frac{(1 + \nu) FM (\theta - \sin\theta)}{E r t \theta_1} \quad (54)$$

Having expressions for the  $\theta$ , or  $V$ , and the radial, or  $U$ , displacements it is possible to solve for the relative displacement between two originally adjacent points after slip has occurred. Figure 15 depicts the quantity that is desired.

The component of the displacement of interest is the  $\theta$  direction or  $V$  component. On one-half of the slip region, region 1, the displacement will be described by equation (54). Denoting equation (54) in that half as

$$V_1 = f(\sigma_r) + g(\tau_{r\theta}) \quad (55)$$

where

$f( )$  is the  $V$  displacement associated with the radial stress

and

$g( )$  is the  $V$  displacement associated with the shear stress

In the other half of the slip region, region 2, the displacement ( $V_2$ ) will be a combination of the displacement associated with the radial stress ( $f( )$ ) and the displacement associated with the friction force acting on that portion of the slip region ( $h( )$ ). This can be written as

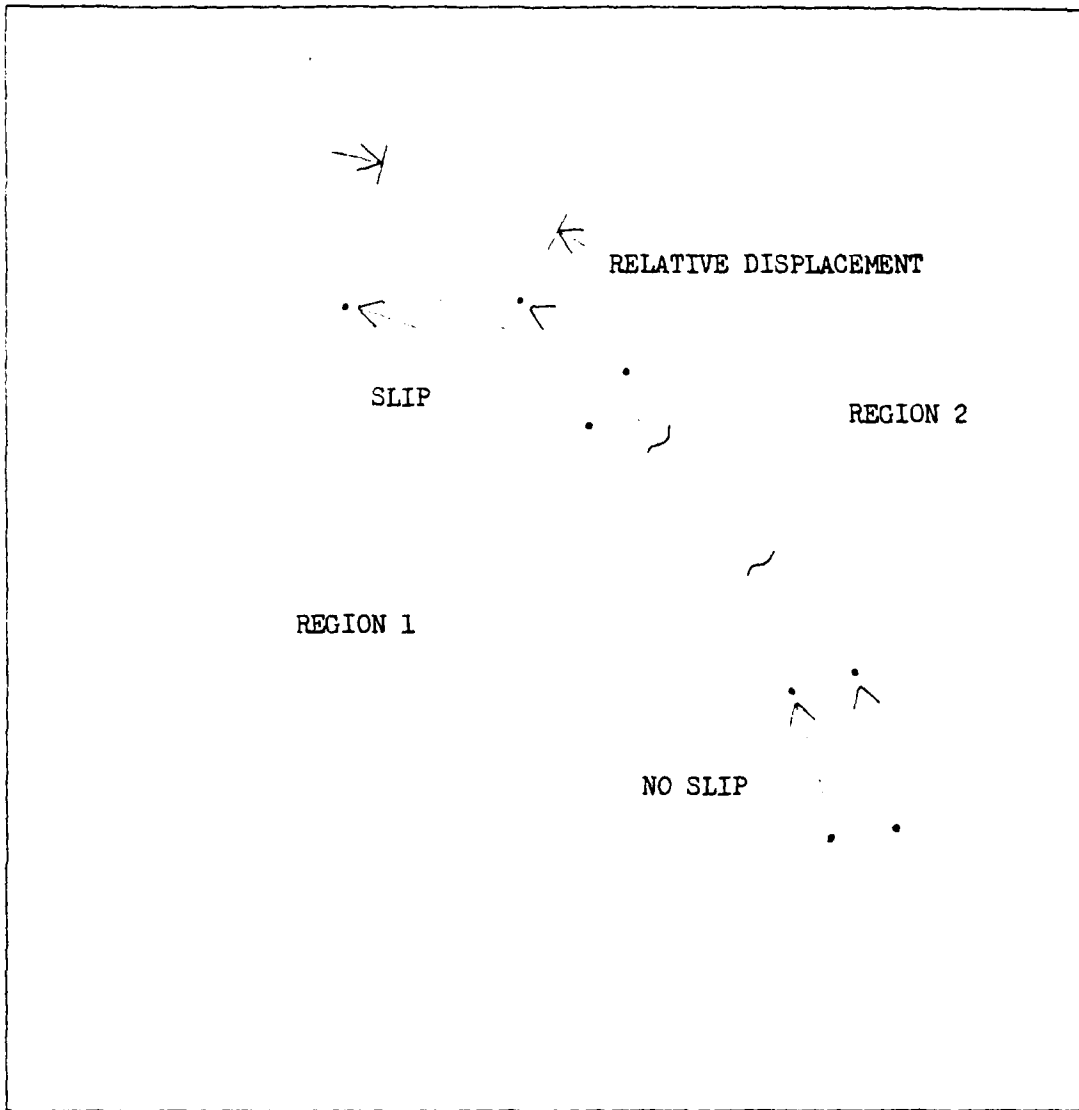


Figure 15. Relative Displacement Across Contact Region

$$v_2 = f(\sigma_r) + h(\mu_D \sigma_r) \quad (56)$$

The relative displacement is the difference between equations (55) and (56)

$$v_1 - v_2 = g(\tau_{r\theta}) - h(\mu_D \sigma_r) \quad (57)$$

which can be written as

$$v_1 - v_2 = \frac{(1 + \nu) F M (\theta - \sin\theta)}{E r t \theta_1} - \frac{\mu_D P(\nu - 1)\theta \sin\theta}{tE(2\theta_1 - \sin 2\theta_1)} \quad (58)$$

$$+ \frac{2(\nu - 1) F \sin\omega T \cos\theta}{tE(2\theta_1 + \sin 2\theta_1)} + \frac{(\nu - 1) F \sin\omega T \theta \sin\theta}{tE(2\theta_1 + \sin 2\theta_1)}$$

Since the energy dissipated is related to the integral, over the slip region, of the friction force times the relative displacement it is necessary to determine the limits of integration.

#### Points of Slip Initiation and Zero Normal Force

There will be two such points (Q and R), one on each side of the blade root, where slip will begin (Figure 14). The equation for the two points where the friction force and the shear stress are equal is

$$-ABS \tau_{r\theta} = \mu_S \sigma_r \quad (59)$$

Solving for points Q and R, the points of equality, on the blade contact surface by writing

$$\mu_S \sigma_r = L \sin\theta + G \cos\theta \quad (60)$$

where

$$L = \frac{2P\mu_S}{rt(\sin 2\theta_1 - 2\theta_1)} \quad (61)$$

$$G = \frac{2F\mu_S \sin\omega T}{rt(\sin 2\theta_1 + 2\theta_1)}$$

and writing

$$- ABS \tau_{r0} = H \quad (62)$$

setting the two functions equal to each other

$$L \sin \theta + G \cos \theta = H$$

rearranging the equation and squaring both sides

$$L^2 (1 - \cos^2 \theta) = G^2 \cos^2 \theta + H^2 - 2HG \cos \theta$$

collecting terms results in a quadratic equation

$$(L^2 + G^2) \cos^2 \theta - 2HG \cos \theta + (H^2 - L^2) = 0 \quad (63)$$

This equation can be solved for the angles corresponding to points Q and R.

Due to the nature of the loading on the blade root there will be a small portion of the contact surface adjacent to the y-axis which will be free of any normal force. This small portion of the contact surface will have an outward normal opposite in direction to the direction of the tangential force discussed as the case two loading condition. To solve for the point (S) where the normal force equals zero,

$$\frac{2P \sin \theta}{rt(\sin 2\theta_1 - 2\theta_1)} = - \frac{2F \sin \omega T \cos \theta}{rt(2\theta_1 + \sin 2\theta_1)} \quad (64)$$

Solving the equality for the angle of the point (S).

$$\theta = \tan^{-1} \frac{F(\sin 2\theta_1 - 2\theta_1)}{P(2\theta_1 + \sin 2\theta_1)} \quad (65)$$

Having an expression for the normal force on the contact surface (equation 18) the friction force can be written as

$$\mu_D \sigma_r = \frac{2P \mu_D \sin \theta}{tr(\sin 2\theta_1 - 2\theta_1)} + \frac{2F \mu_D \sin \omega T \cos \theta}{tr(\sin 2\theta_1 - 2\theta_1)} \quad (66)$$

The relative displacement across the contact surface due to slip is known (equation 58), and the points of slip initiation are known

(equation 65). With these expressions the energy dissipated due to slip can be calculated.

#### Energy Dissipated by Slip

The energy dissipated by the slip region is the product of the friction force acting over the region times the relative displacement across the interface. This quantity, integrated over the slip region, will give the amount of energy dissipated at a particular instant. Integrating this result over one cycle will result in the energy dissipated per cycle. During one cycle the exciting force will change from zero to a maximum value four times. Thus the energy dissipated per cycle ( $D_o$ , lb-in) is

$$D_o = 4 \int_{\text{slip region}} \text{Friction force} \times \text{Relative displacement} \quad (67)$$

Four times the product of equations (66) and (58) integrated over the slip region gives the energy dissipated per cycle.

$$D_o = 4 \left[ \int_0^Q (\mu_D \sigma_R) (V_1 - V_2) d\theta + \int_R^\pi (\mu_D \sigma_R) (V_1 - V_2) d\theta \right] \quad (68)$$

It should be noted that the region of zero normal force is included in the above expression. The region is on the order of two degrees and its inclusion in the expression has a negligible effect.

In order to isolate the effect of the slip damping it is necessary to develop expressions for the air damping and the material damping.

#### Energy Dissipated By Air Damping

The amplitudes associated with the blade displacements are small and thus the force acting on the blade is proportional to velocity (reference 2)

$$F = CV \quad (69)$$

utilizing references (2) and (5) the equation for the air damping of the blade is

$$D_o = \pi C_7 \omega^2 X^2 \quad (70)$$

where

$\omega$  is the circular frequency of the blade

$X$  is the displacement of a point on the blade

and  $C_7$  is a constant equal to

$$C_7 = \frac{1}{2} \rho S C_D \quad (71)$$

where

$\rho$  is the density for air

$S$  is the wetted area of the blade

$C_D$  is the drag coefficient for the blade

the expression for the energy dissipated can be written

$$D_o = \frac{\pi}{2} \rho S C_D \omega^2 X^2 \quad (72)$$

#### Energy Dissipated By Hysteresis Damping

To develop an expression for the hysteresis damping of the blade, a relationship between stress and energy dissipated of the form

$$D = J \sigma_B^N \quad (73)$$

was assumed.  $J$  and  $N$  are empirically derived constants and  $\sigma_B$  is the bending stress due to the tip load on the blade.  $D$  has units of (lb-in/in<sup>3</sup>) and must be integrated over the total volume of the blade to obtain the energy dissipated

$$D_o = \int_0^t \int_{-b/2}^{b/2} \int_0^L J \left[ \frac{MY}{I} \right]^N dx dy dz \quad (74)$$

Evaluating this integral where  $M = F(L - X)$  leads to

$$D_o = \frac{2Jt}{(N + 1)^2} \left(\frac{F}{I}\right)^N \left(\frac{bL}{2}\right)^{N+1} \quad (75)$$

For Inconel-X and  $\sigma_B$  less than 33 KSI

$$\begin{aligned} N &= 2.224 \\ J &= 4.586 \times 10^{-13} \end{aligned} \quad (76)$$

In order to be able to use the experimental model to verify the analytical model, it is necessary to develop an expression which relates such quantities as blade tip displacement, exciting force, clamping pressure, material properties, etc. This can be done by developing a solution to the equation of motion for the blade. The first step toward this is the evaluation of the restoring moment due to slip which acts on the blade root.

#### Restoring Moment Due to Slip

The restoring moment due to slip ( $M$ ) can be calculated from

$$M = r^2 \int \left[ \int \mu_D \sigma_r d\theta + \int \mu_D \sigma_r d\theta \right] dz \quad (77)$$

where  $t$  is the depth of the blade root in the  $z$  direction. Placing equation (18) into equation (69) and evaluating,

$$M = r\mu_D \left[ \frac{-2P}{(\sin 2\theta_1 - 2\theta_1)} \left[ \cos\theta \Big|_0^Q + \cos\theta \Big|_R^\pi \right] + \frac{2F \sin\omega T}{(2\theta_1 + \sin 2\theta_1)} \left[ \sin\theta \Big|_0^Q + \sin\theta \Big|_R^\pi \right] \right]$$

This leads to an expression for the restoring moment,

$$M = r\mu_D \left[ \frac{2P(\cos R - \cos Q - 2)}{(\sin 2\theta_1 - 2\theta_1)} + \frac{2F \sin\omega T(\sin Q - \sin R)}{(2\theta_1 + \sin 2\theta_1)} \right] \quad (78)$$

which can be rewritten as

$$M = m \sin \omega T$$

where

$$m = r \mu_D \left[ \frac{2P(\cos R - \cos Q - 2)}{(\sin 2\theta_1 - 2\theta_1) \sin \omega T} + \frac{2F(\sin Q - \sin R)}{(2\theta_1 + \sin 2\theta_1)} \right] \quad (79)$$

It should be noted that the region of zero normal force was included in the determination of the restoring moment which was due to friction developed on the contact surface. The region is on the order of two degrees and its inclusion in the integration has a negligible effect on the result.

#### Equation of Motion and Boundary Conditions

To derive the equation of motion and boundary conditions for the blade, Hamilton's principle was used.

$$\int_0^T (\delta K - \delta U + \delta W) dT = 0 \quad (80)$$

For the blade the variation of the kinetic energy is

$$\delta K = \int_0^L \gamma \frac{\partial W}{\partial T} \frac{\partial}{\partial T} \delta W dx + I_0 \left. \frac{\partial^2 W}{\partial x \partial T} \right|_{x=0} \frac{\partial^2}{\partial x \partial T} \delta W \Big|_{x=0} \quad (81)$$

where

$L$  is the length of the blade in inches

$\gamma$  is the mass per unit length of the blade (lbm/in)

$I_0$  is the mass moment of inertia of the blade root about point 0 (lbm-in<sup>2</sup>)

$W = W(x, T)$  is the displacement of the blade in the  $Y$  direction

The variation of the potential energy of the blade is

$$\delta U = \int_0^L EI \frac{\partial^2 W}{\partial x^2} \frac{\partial^2}{\partial x^2} \delta W dx \quad (82)$$

where

$E$  is the modulus of elasticity of the blade (lbf/in<sup>2</sup> =  
386 lbm/sec-in)

$I$  is the area moment of inertia of the blade (in<sup>4</sup>)

and the variation in the work is

$$\delta WK = F \sin \omega T \delta W \Big|_{x=L} - m \sin \omega T \frac{\partial}{\partial x} \delta W \Big|_{x=0} \quad (83)$$

Placing equations (81), (82), and (83) into equation (80), performing the necessary integrations, and eliminating the zero terms leads to the equation of motion,

$$EI \frac{\partial^4 W}{\partial x^4} + \gamma \frac{\partial^2 W}{\partial T^2} = 0 \quad (84)$$

the boundary conditions at  $x=0$ ,

$$W(0,T) = 0 \quad (85)$$

and

$$EI \frac{\partial^2}{\partial x^2} W(0,T) + \frac{\partial^2}{\partial t^2} \left[ \frac{\partial}{\partial x} W(0,T) \right] I_0 + m \sin \omega T = 0 \quad (86)$$

and the boundary conditions at  $x = L$

$$EI \frac{\partial^2}{\partial x^2} W(L,T) = 0 \quad (87)$$

and

$$EI \frac{\partial^3}{\partial x^3} W(L,T) + F \sin \omega T = 0 \quad (88)$$

#### Solution to Equation of Motion

To solve the equation of motion for the displacement it is necessary to make the boundary conditions homogeneous. Denoting

$$\frac{\partial W}{\partial x} = W_x ; \quad \frac{\partial^2 W}{\partial x^2} = W_{xx} ; \quad \text{etc.}$$

and writing the equation of motion

$$W_{xxxx} - a^4 W_{tt} = 0 \quad (89)$$

where

$$-a^4 = \frac{Y}{EI} \quad (90)$$

Making a change of variables

$$W(x,T) = Y(x,T) + (B_1 \sin a \psi x + B_2 \cos a \psi x + B_3 \sinh a \psi x + B_4 \cosh a \psi x) \sin \psi^2 T \quad (91)$$

with

$$\psi^2 = \omega$$

From equation (91), and the boundary condition (85) for

$$W(x,T) = Y(x,T) = 0$$

$$B_4 = -B_2$$

Placing the result in equation (91) and substituting this into equation (87) and requiring that

$$W_{xx}(L,T) = Y_{xx}(L,T) = 0$$

requires that

$$B_3 \sinh a \psi L = B_1 \sin a \psi L + B_2 (\cos a \psi L + \cosh a \psi L) \quad (92)$$

Using equation (88) and forcing

$$W_{xxx}(L,T) = Y_{xxx}(L,T) = 0$$

requires that

$$B_1 \cos a \psi L - B_2 (\sin a \psi L - \sinh a \psi L) - B_3 \cosh a \psi L = \frac{F}{EI a^3 \psi^3} \quad (93)$$

Using equation (86) and forcing

$$EI W_{xx}(0,T) + I_0 W_{xtt}(0,T) = EI Y_{xx}(0,T) + I_0 W_{xtt}(0,T) = 0$$

requires that

$$B_2 = \frac{m - I_0 a \psi^5 (B_1 + B_3)}{2EI a^2 \psi^2} \quad (94)$$

Equations (92), (93), and (94) provide three equations in three unknowns which can be solved to provide the following results,

$$B_1 = \left[ \frac{m}{I_0 \psi^5 a} - \frac{F}{EI a^3 \psi^3 (\cos \psi L - \coth \psi L \sin \psi L)} \left[ 1 + \frac{\sin \psi L}{\sinh \psi L} \right] \right] \times \left[ 1 + \frac{\sinh \psi L}{\sin \psi L} + \left[ 1 + \frac{\sin \psi L}{\cos \psi L + \cosh \psi L} \right] \right] \times \left[ \frac{(\sin \psi L - \sinh \psi L) - (\cos \psi L + \cosh \psi L) \coth \psi L}{\cos \psi L - \coth \psi L \sin \psi L} \right] + \frac{F}{EI a^3 \psi^3 (\cos \psi L - \coth \psi L \sin \psi L)} \quad (95)$$

$$B_2 = \left[ \frac{m}{I_0 \psi^5 a} - \frac{F}{EI a^3 \psi^3 (\cos \psi L - \coth \psi L \sin \psi L)} \left[ 1 + \frac{\sin \psi L}{\sinh \psi L} \right] \right] \times \left[ \frac{\cos \psi L - \coth \psi L \sin \psi L}{(\sin \psi L - \sinh \psi L) - (\cos \psi L + \cosh \psi L) \coth \psi L} \right] \times \left[ 1 + \frac{\sinh \psi L}{\sin \psi L} + \frac{\sin \psi L}{\cos \psi L + \cosh \psi L} + 1 \right] \quad (96)$$

$$B_3 = \left[ \frac{[(\sin \psi L - \sinh \psi L) - (\cos \psi L + \cosh \psi L) \coth \psi L] \sin \psi L}{(\cos \psi L - \coth \psi L \sin \psi L) \sinh \psi L} + \frac{(\cos \psi L + \cosh \psi L)}{\sinh \psi L} \right] \left[ B_2 \right] + \frac{F \sin \psi L}{EI a^3 \psi^3 (\cos \psi L - \coth \psi L \sin \psi L) \sinh \psi L} \quad (97)$$

With the change in variables, and the constants (95), (96), and (97)

the homogeneous equation of motion is

$$Y_{xxxx} + \frac{Y}{EI} Y_{tt} = 0 \quad (98)$$

and the homogeneous boundary conditions are

$$Y(0, T) = 0 \quad (99)$$

$$Y_{xx}(L, T) = 0 \quad (100)$$

$$Y_{xxx}(L, T) = 0 \quad (101)$$

$$EI Y_{xx}(0, T) + I_0 Y_{xtt}(0, T) = 0 \quad (102)$$

Assuming a solution of equation (98) of the form

$$Y(x,T) = X(x)Z(T)$$

and using the solution method of separation of variable results in

$$Z(T) = J\cos\hat{\omega}T + K\sin\hat{\omega}T \quad (103)$$

and

$$X(x) = D_1\sin\beta x + D_2\cos\beta x + D_3\sinh\beta x + D_4\cosh\beta x \quad (104)$$

where

$$\beta^4 = \frac{\hat{\omega}^2 Y}{EI} \quad (105)$$

Using the first boundary condition (99)

$$D_2 = -D_4 \quad (106)$$

Using the second boundary condition (100)

$$-D_1\sin\beta L + D_4(\cos\beta L + \cosh\beta L) + D_3\sinh\beta L = 0 \quad (107)$$

Using the third boundary condition (101)

$$-D_1\cos\beta L + D_4(\sinh\beta L - \sin\beta L) + D_3\cosh\beta L = 0 \quad (108)$$

Using the fourth boundary condition (102), rewritten as

$$X_{xx}(0) - \frac{I\hat{\omega}^2}{EI} X_x(0) = 0$$

gives

$$2D_4 - \frac{I\hat{\omega}^2}{EI\beta} (D_1 + D_3) \quad (109)$$

For the non-trivial solution where  $D_1$ ,  $D_2$ ,  $D_3$ , and  $D_4$  are not zero, the determinant of the coefficient matrix must be zero. The governing equation is

$$\frac{I\hat{\omega}^2}{EI\beta} (\cosh\beta L \cos\beta L + 1) + \cos\beta L \sinh\beta L - \sin\beta L \cosh\beta L = 0 \quad (110)$$

This equation can be solved, to provide the values of  $\beta L$  and  $\hat{\omega}$ , using

$$\hat{\omega} = \left[ \frac{(\beta L)^4 EI}{\gamma L^4} \right]^{1/2} \quad (111)$$

See Appendix A for the solutions to (110) and (111). Using equations (107), (108), and (109), the constants  $D_3$  and  $D_4$  can be put in terms of  $D_1$  to provide

$$D^3 = D_1 \left[ -\frac{I_0(\beta L)^3}{2L^3 \gamma} \frac{(\cos\beta L + \cosh\beta L)}{\sinh\beta L} - 1 + \frac{\sin\beta L}{\sinh\beta L} + \frac{2L^3 \gamma}{I_0(\beta L)^3} \frac{\sin\beta L}{(\cos\beta L + \cosh\beta L)} \right] \quad (112)$$

and

$$D_4 = D_1 \left[ -\frac{1}{4} \left[ \frac{I_0(\beta L)^3}{\gamma L^3} \right]^2 \frac{(\cos\beta L + \cosh\beta L)}{\sinh\beta L} + \frac{I_0(\beta L)^3}{2L^3 \gamma} \frac{\sin\beta L}{\sinh\beta L} + \frac{\sin\beta L}{(\cos\beta L + \cosh\beta L)} \right] \quad (113)$$

Setting  $D_1 = 1$  and substituting (112), (113), and (106) into equation (104) provides,

$$x_N(x) = \sin\beta_N x + \left[ -\frac{1}{4} \left[ \frac{I_0(\beta_N L)^3}{\gamma L^3} \right]^2 \frac{(\cos(\beta_N L) + \cosh(\beta_N L))}{\sinh(\beta_N L)} + \frac{I_0(\beta_N L)^3}{2L^3 \gamma} \frac{\sin(\beta_N L)}{\sinh(\beta_N L)} + \frac{\sin(\beta_N L)}{(\cos(\beta_N L) + \cosh(\beta_N L))} \right] \times (\cosh\beta_N x - \cos\beta_N x) + \left[ -\frac{I_0(\beta_N L)^3}{2L^3 \gamma} \frac{(\cos(\beta_N L) + \cosh(\beta_N L))}{\sinh(\beta_N L)} - 1 + \frac{2L^3 \gamma}{I_0(\beta_N L)^3} \frac{\sin(\beta_N L)}{(\cos(\beta_N L) + \cosh(\beta_N L))} + \frac{\sin(\beta_N L)}{\sinh(\beta_N L)} \right] (\sinh\beta_N x) \quad (114)$$

Using equations (114) and (103), the solution to equation (98) can be

written,

$$Y(x,T) = \sum_{N=1}^{\infty} X_N(x) (J_N \cos \hat{\omega}_N T + K_N \sin \hat{\omega}_N T) \quad (115)$$

Substituting the above into equation (91) provides an expression for the displacement.

$$W(x,T) = \sum_{N=1}^{\infty} X_N(x) (J_N \cos \hat{\omega}_N T + K_N \sin \hat{\omega}_N T) + \left[ B_1 \sin a \psi x + B_2 (\cos a \psi x - \cosh a \psi x) + B_3 \sinh a \psi x \right] \sin(\psi^2 T) \quad (116)$$

To evaluate the remaining constants  $J_N$  and  $K_N$  it is necessary to use the initial conditions

$$W(x,0) = 0 \quad (117)$$

and

$$W_t(x,0) = 0 \quad (118)$$

The first initial condition (117) requires  $J_N = 0$ . Using this result and the second initial condition (118) requires that

$$\sum_{N=1}^{\infty} K_N \hat{\omega}_N X_N(x) = -\psi^2 (B_1 \sin a \psi x + B_2 (\cos a \psi x - \cosh a \psi x) + B_3 \sinh a \psi x) \quad (119)$$

The functions  $\hat{\omega}_N X_N$  are not orthogonal functions. Therefore a collocation method must be used to solve for the constants ( $K_N$ ). The desired number of modes (N) must be chosen, and the  $X_N(x)$  as well as the right hand function must be evaluated at a number of points along the blade. The  $X_N(x)$  can be evaluated using equation (110) and the right hand function is evaluated using equations (95), (96), and (97). A matrix expression is developed

$$\left[ \text{constants} \right] \begin{pmatrix} K_1 \\ \vdots \\ K_N \end{pmatrix} = \begin{pmatrix} f_1(x) \\ \vdots \\ f_N(x) \end{pmatrix} \quad (120)$$

which can be solved for the  $K_N$ 's.

The solution to the equation of motion provides an expression which relates the various parameters of the experimental and analytical models. This expression can be used as a means of verifying the analytical model with the experimental model. It can also be used to study the effects of varying the different parameters. If there is correlation between the analytical model and the experimental model, then the expressions for the energy dissipated can be assumed to be correct.

#### IV. Recommendations

The recommendations are put forth in hopes that some useful information, regarding slip damping of Turbine/Compressor blades, can be generated, using the analytical and experimental models provided by this study.

1) Using the analytical model the following quantities for various combinations of exciting force and clamping pressure should be generated:

- a) Value of exciting force for complete slip.
- b) The exciting force necessary to obtain a set blade tip displacement.
- c) A comparison of the energy being dissipated by the three forms of damping.

2) Using the experimental model

- a) A wider variation of clamping pressures and exciting force.
- b) Differing conditions for the contact surface, such as a sandwiched viscoelastic layer.
- c) Investigations of slip in an environment with an elevated temperature.

3) The analytical model should be modified to include a sandwiched viscoelastic layer at the contact surface.

### Bibliography

1. Alspaugh, D.W. "Analysis of Coulomb Friction Vibration Dampers." Journal of Sound and Vibration. 57(1)(1978): 65-78.
2. Baker, Wilfred E., William E. Woolam, and Dana Young. Air and Internal Damping of Thin Cantilever Beams. U.S. Army Research Office - Durham, DDC Publication AD664408, 1967.
3. Boyce, William E., and Richard C. Dippima. Elementary Differential Equations and Boundary Value Problems. 2nd Ed. New York: John Wiley and Sons, Inc., 1969.
4. Edstrom, Clarence R. "A Boundary Value Problem." Mathematics Magazine. Vol. 45, No. 3 (1972): 149-150.
5. Goodman, L.E. "A Review of Progress in Analysis of Interfacial Slip Damping." in Structural Damping, ed. Jerome E. Ruzicka, ASME Colloquium, Atlantic City, N.J.: December 1959.
6. Goodman, L.E., and J.H. Klumpp. "Analysis of Slip Damping with Reference to Turbine Blade Vibration." Journal of Applied Mechanics, Vol. 23 (1956): 421-429.
7. Gorlov, V.B. The Investigation of Stresses in a Compressor Blade Foil. FTD Translation, MT-24-12-72, DDC Publication AD750497.
8. Hanson, M.P., A.J. Meyer, JR., and S.S. Manson. "A Method of Evaluating Loose-Blade Mounting as a Means of Suppressing Turbine and Compressor Blade Vibration." SESA Proceedings, Vol. X No. 2 (November 1950): 103-116.
9. Harris, Cyril M., and Charles E. Crede, ed. Shock and Vibration Handbook, 2nd ed. New York: McGraw-Hill Book Company, 1976.
10. Jones, D.I.G. "Vibrations of a Compressor Blade with Slip at the Root." unpublished report, January 1978.
11. Jones, D.I.G., and Agnieszka Muszynska. "Effect of Slip on Response of a Vibrating Compressor Blade." ASME paper 77-WA-GT-3: ASME, November 1977.
12. Klumpp, James H., and Benjamin J. Lazan. Frictional Damping and Resonant Vibration Characteristics of an Axial Slip Lap Joint. WADC Technical Report 54-64, 1954.
13. Lee, L.T. A Graphical Compilation of Damping Properties of Both Metallic and Non-Metallic Materials. AFML-TR-66-169, 1966.
14. Little, Robert Wm. Elasticity. New Jersey: Prentice-Hall Inc., 1973.
15. McBain, James C., and J. Genin. Optimum Support Damping for a Vibrating Beam. AFAPL-TR-76-14, DDC Publication ADA025106, 1976.

16. Meirovitch, Leonard. Analytical Methods in Vibrations. London: Collier-Macmillan Limited. 1967.
17. Michell, J.H. "Elementary Distributions of Plane Stress." London Math. Soc. Proceedings, Vol. XXXII (1900): 35-61.
18. Plunkett, R. "Measurement of Damping." in Structural Damping, ed. Jerome E. Ruzicka, ASME Colloquium, Atlantic City, M.J.: December 1959.
19. Radomski, M.A., and J.F. Wasserman. Investigation of Failure of Compressor Disk Post Platform and Blade in GE4 Kit Engine. General Electric Company, DDC Publication AD881506L, 1970.
20. Sadighi, B. "An Analysis of Root Flexibility Effects on Turbine Blade Vibration Characteristics," Master's Thesis, Imperial College London, 1977.
21. Snowdon, J.C. Vibration and Shock in Damped Mechanical Systems. New York: John Wiley and Sons, Inc., 1968.
22. Sridharan, Prabha. Damping in Porcelain Enamel Coatings. AFML TR-74-191, DDC Publication AD A031774: 1976.
23. Timoshenko, S.P., and J.N. Goodier. Theory of Elasticity. New York: McGraw-Hill Book Company, 1970.
24. Torvik, Peter J. "Damping: Its Application in Transportation Vehicles." in Materials on the Move, Vol. 6, National SAMPE Technical Conference Series, 1974.
25. Volterra, Enrico, and E.C. Zachmanoglou. Dynamics of Vibrations. Columbus, Ohio: Charles E. Merrill Books, Inc., 1965.

## Appendix A

### Solution To Characteristic Equation

The characteristic equation

$$\frac{I_o \hat{\omega}^2}{EI} (\cosh\beta L \cos\beta L + 1) + \cos\beta L \sinh\beta L - \sin\beta L \cosh\beta L = 0 \quad (A-1)$$

can be solved using a combination of the bisection and secant methods to find the points ( $\beta_N L$ ) where equation (A-1) is satisfied. Using the relation

$$\hat{\omega}^2 = \frac{\beta^4 EI}{\gamma} \quad (A-2)$$

and the values

$$L^3 = 1157.625 \text{ in}^3$$

$$I_o = .01828 \text{ lbm-in}^2$$

$$\gamma = .18625 \frac{\text{lbm}}{\text{in}}$$

The first five values of  $\beta L$  which satisfy equation (A-1) are listed in column two of Table One. In column three of the same table are listed the classic values of  $\beta L$  for a clamped-pinned beam. Using equation (A-2) the frequencies corresponding to the different values of  $\beta L$  are entered in column four of Table One.

TABLE ONE

N	EIGENVALUES		ANALYTICAL MODEL CPS
	ANALYTICAL BLADE MODEL VALUES	CLAMPED-PINNED BEAM VALUES	
$\beta_1^L$	3.9290282	3.9266023	322.513
$\beta_2^L$	7.0834600	7.0685827	1048.256
$\beta_3^L$	10.2538495	10.2101761	2196.598
$\beta_4^L$	13.4449040	13.3517688	3776.523
$\beta_5^L$	16.4500000	16.4933614	5653.384

Table One. Eigenvalues an Corresponding Frequencies for Equation (61)

## Appendix B

### Accelerometer and Impedance Head Calibration

Figure 16 shows the set-up used to calibrate the accelerometer and force gage. The large MB model C10 exciter and the MB model 3402MB amplifier were used. The accelerometer and the force gage were attached to the head of the exciter. A known mass was placed over the impedance head. The signals from the accelerometer and the force gage were fed thru the same data chain as was used for the data taking. A known acceleration was exerted by the exciter. The output of the accelerometer and the force gage were recorded. Knowing the mass over the force gage allowed the calculation of the force corresponding to a certain signal level.

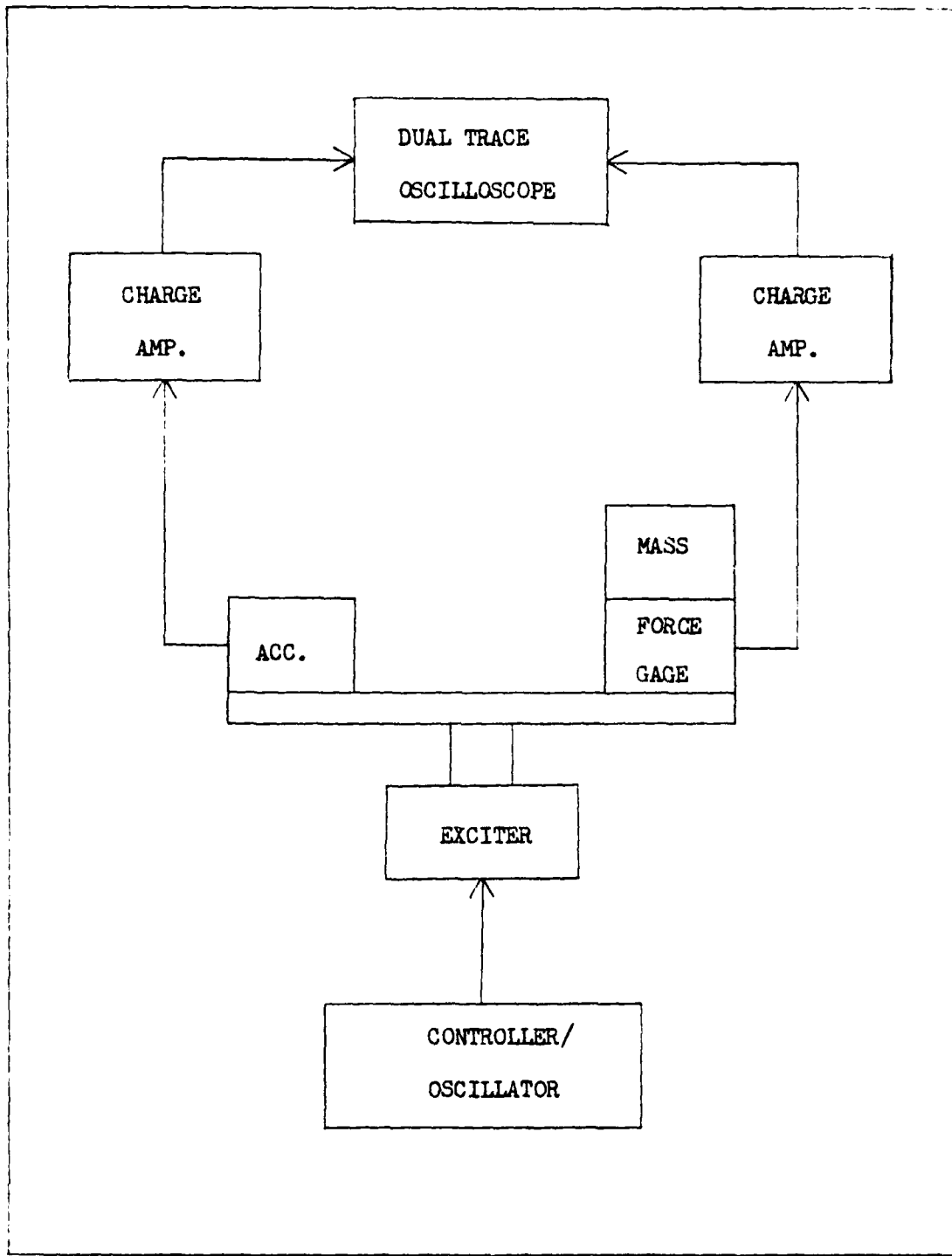


Figure 16. Schematic of Calibration Set-up for the Accelerometer and Impedance Head Calibration

## Appendix C

### Spring Beam Calibration

To calibrate the spring beam it was necessary to apply a known force and record the corresponding signal from the strain gages. Figure 17 shows the force table and guide which, when assembled on the disk model (Figure 18), allowed a known force to be applied to the spring beam. Increasing amounts of weight were set on the force table and the signal from the strain gages was recorded.

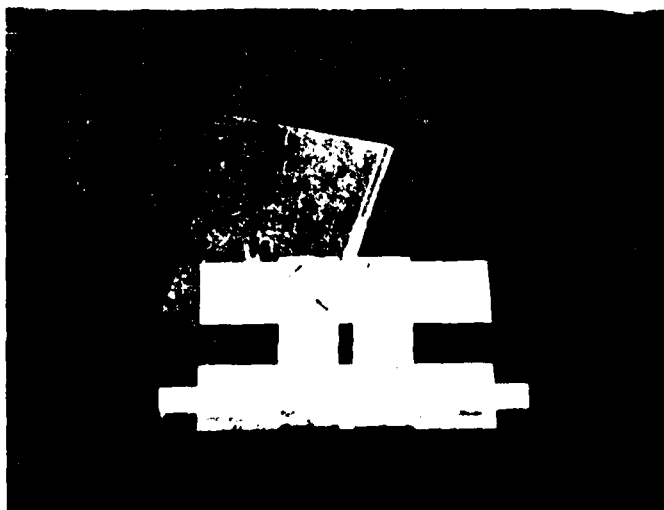


Figure 17. Picture of Force Table and Guide

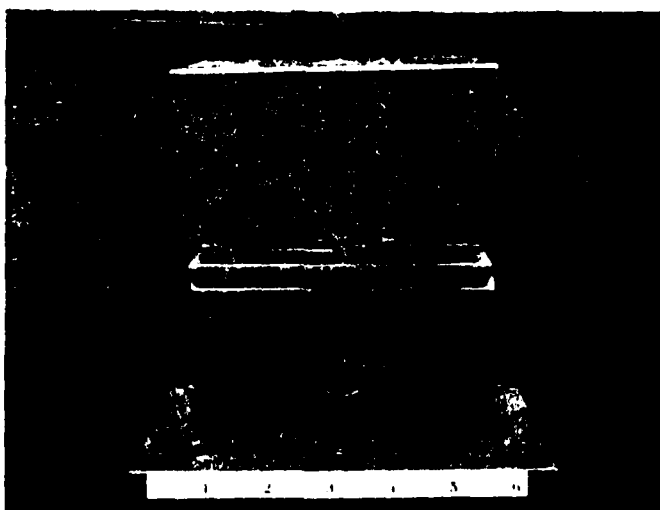


Figure 18. Picture of Force Table in Place on the Disk Model

Vita

Michael Charles Kimberling was born on 7 February 1951 in Los Angeles, California. He graduated from high school in Anaheim California in 1969 and was accepted to the U.S. Air Force Academy. Upon graduation in June 1973, he received a commission in the USAF and the Degree of Bachelor of Science in Engineering Mechanics. He was assigned as a Division Mechanical Engineer to the Air Force Weapons Laboratory, Kirtland AFB, NM. He entered the School of Engineering, Air Force Institute of Technology, in June 1977.

Permanent address: 913 LaMark LN

Anaheim, California 92802

REPORT DOCUMENTATION PAGE		READ INSTRUCTIONS BEFORE COMPLETING FORM
1. REPORT NUMBER AFIT/GAE/AA/78D-11	2. GOVT ACCESSION NO.	3. RECIPIENT'S CATALOG NUMBER
4. TITLE (and Subtitle)  SLIP DAMPING OF TURBINE BLADES	5. TYPE OF REPORT & PERIOD COVERED  MS Thesis	
7. AUTHOR(s)  Michael C. Kimberling	6. PERFORMING ORG. REPORT NUMBER	
9. PERFORMING ORGANIZATION NAME AND ADDRESS  Air Force Institute of Technology (AFIT/EN) Wright-Patterson AFB, Ohio 45433	8. CONTRACT OR GRANT NUMBER(s)	
11. CONTROLLING OFFICE NAME AND ADDRESS	10. PROGRAM ELEMENT, PROJECT, TASK AREA & WORK UNIT NUMBERS	
14. MONITORING AGENCY NAME & ADDRESS (if different from Controlling Office)	12. REPORT DATE December, 1978	13. NUMBER OF PAGES 53
	15. SECURITY CLASS. (of this report) Unclassified	15a. DECLASSIFICATION/DOWNGRADING SCHEDULE
16. DISTRIBUTION STATEMENT (of this Report)  Approved for public release; distribution unlimited		
17. DISTRIBUTION STATEMENT (of the abstract entered in Block 20, if different from Report)		
18. SUPPLEMENTARY NOTES  Approved for public release; IAW AFR 190-17 Joseph P. Hipps, Major, USAF Director of Information		
19. KEY WORDS (Continue on reverse side if necessary and identify by block number) Slip Damping Turbine Blades Compressor Blades Damping		
20. ABSTRACT (Continue on reverse side if necessary and identify by block number)  An experimental, and an analytical, model of Turbine/Compressor blade with a circular root geometry is developed for the purpose of studying the effects of slip damping on the response of the blade. The expression for the energy dissipated by slip damping is presented. In addition the expressions for the energy dissipated by air and hysteresis damping are presented. The equation of motion for the blade is developed, and solved,		

SECURITY CLASSIFICATION OF THIS PAGE(When Data Entered)

to provide an expression relating the various parameters of the experimental and analytical models.

SECURITY CLASSIFICATION OF THIS PAGE(When Data Entered)